Received: 1 November 2019 | Revised: 15 March 2020 | Accepted: 25 March 2020

DOI: 10.1002/pc.25590

REVIEW ARTICLE

spe INSPIRING PLASTICS PROFESSIONALS Polymer COMPOSITES WILEY

The effect of filler localization on the properties of biopolymer blends, recent advances: A review

Mokgaotsa J. Mochane[1] | **Jeremia S. Sefadi**[2] | **Teboho S. Motsoeneng**[3] | **Tilsetso E. Mokoena**[1] | **Tladi G. Mofokeng**[4] | **Teboho C. Mokhena**[5,6]

[1]Department of Life Sciences, Central University of Technology, Bloemfontein, Free State, South Africa

[2]Department of Physical and Earth Sciences (PES), Sol Plaatje University, Kimberley, South Africa

[3]Department of Chemistry, University of South Africa, Florida Park, Gauteng, South Africa

[4]DST/CSIR National Centre for Nanostructured Materials, Council for Scientific and Industrial Research, Pretoria, South Africa

[5]Advanced Polymer Composites, Centre of Nanostructured and Advanced Material, CSIR, Pretoria, South Africa

[6]Department of Chemistry, Nelson Mandela University, Port Elizabeth, South Africa

Correspondence
Mokgaotsa J. Mochane, Department of Life Sciences, Central University of Technology, Free State, Private Bag X20539, Bloemfontein 9300, South Africa.
Email: mochane.jonas@gmail.com

Funding information
National Research Foundation

Abstract

In recent times, the field of biopolymer (BP) blends has been the focus of intensive fundamental and applied researches. Such BP combinations possess unique properties that are different from those of the individual components. However, most polyester polymers are thermodynamically immiscible because of their poor interactions. In the past, a third component, known as a well-defined diblock or triblock copolymer, whose chemical structure is identical to that of the main components, was usually used as a compatibilizer in order to emulsify the interfacial phase, decreasing the interfacial tension and refining the phase size. Currently, nanofillers are used to improve the phase morphologies of immiscible BP blends. The main advantage of using nanofillers, when compared to copolymers, is that the former can simultaneous act as nano-reinforcements and compatibilizers. In this review, the addition of nanofillers as the third component in the BP blend systems are reported in relation to their morphologies, barrier properties, shape memory, thermal, and mechanical properties. The effects of selectively localized nanofillers on the properties of the BP blends are also explored, with the aim of establishing the relationships between the localization of the fillers and the overall properties of the BP blends. Furthermore, the effect of the processing techniques on the localization of the nanofillers/BP blend is also reported. The review article discusses recent progress from 2014 up to 2019 on filler localization of BP blend nanocomposites.

KEYWORDS

biodegradable, biopolymers, chitosan, compatibilization, fillers

1 | INTRODUCTION

Recently, biopolymers (BPs) and their various systems have been widely reported in the literature review as an alternative to petroleum-based synthetic polymers.[1] BPs are polymers produced from natural sources either chemically synthesized from biological material or entirely biosynthesized by living organisms. This has resulted in a multitude of healthcare products on the market that use BPs in their formulations as a functional excipient or even as an active ingredient. Their diverse compositions, tunable physical behavior, and a wide variety of choice have fuelled the interest in BPs. These natural raw materials are in abundance, recyclable, biodegradable and relatively positive ecological footprint, making them attractive feedstocks for bioplastics, a new generation of

environmentally friendly plastics utilized in several industrial applications.[1–7] In addition, their renewable nature make this class of materials attractive to high-value sectors such as the pharmaceutical and biomedical industries.

However, a far-reaching use of BPs is often constrained by the necessary improvement of some functional properties such as mechanical, thermal, and barrier properties. Therefore, intense efforts have been made to improve their physical properties in order to enhance the commercial potential of BPs such as poly(lactic acid) (PLA), poly(caprolactone) (PCL), poly(butylene adipate terephthalate) (PBAT), polyhydroxyalkanoates (PHAs), starch, gelatin, soy protein, casein, and triglycerides.[8–11] Synthetic biodegradable polyesters are considered to be the most commercially competitive polymers because they are producible in a cost-effective manner with a wide range of characteristics. Polyesters are also biocompatible, and biodegradable polymers, these physiochemical features enable their use in a broad range of medical applications that include medical devices such as sutures, plate, bone fixation devices, stent, screws, and tissue repairs.[12–15] Polyesters are also used commercially as drug delivery vehicles.[16,17]

This review intends to provide an overview of the chemical and physical properties of the BP blends/filler nanocomposites and how these nanofillers are localized on the phases of the BP blends systems. In this review article, the applications, surface modifications and processing methods of the most commonly used polyester will be covered.

2 | TYPES OF BIOPOLYMERS

2.1 | Poly(butylene adipate terephthalate)

PBAT is a highly flexible and 100% biodegradable synthetic polymer based on fossil resources.[18] This synthetic BP is prepared by transesterification reaction under controlled conditions, and therefore generally exhibit predictable and reproducible properties.[19] It can be used in several applications, such as packaging materials (trash bags, food containers, film wrapping), hygiene products (diaper back sheets, cotton swabs), biomedical fields, and industrial composting.[20–22] Biodegradation of PBAT depends on its chemical structure and environmental degrading conditions.[19,23] In some cases, the biodegradation occurs by the enzymatic action of microorganisms such as bacteria, fungi, and algae which are present in the natural environment.[20] In other cases, biodegradation occurs by a combined depolymerization process where the polymer chain breaks down by non-enzymatic reaction (eg, chemical hydrolysis, and thermal degradation) and metabolization of these intermediates by microorganisms.[21] Although it is a requirement, the biodegradability of PBAT alone is not enough for consumer acceptance of this material. High production costs and inferior thermophysical and mechanical resistance, when compared with non-BPs, are obstacles that hinder the use of this biodegradable material.[20] As a consequence, the development of a PBAT market will only be attractive when production costs decrease and when their properties are improved.[19]

In general, polyesters are synthesized by polycondensation from combinations of diols and dicarboxylic acids. PBAT, specifically, can be produced by polycondensation reaction of 1,4-butanediol with both adipic and terephthalic acids (or butylene adipate). The preparation of PBAT requires long reaction time, high vacuum, and temperatures usually higher than 190°C. These conditions are required to favour condensation reactions and remove the lighter molecules (water) as a product.[24]

The Young's modulus of PBAT is 20 to 35 MPa, while its tensile strength is in the range of 32 to 36 MPa. Moreover, it is a flexible polymer with an elongation at break of approximately 700% which is higher than most biodegradable polyesters such as PLA and polybutylene succinate.[25] These properties of PBAT are comparable to those of low-density polyethylene (LDPE) thus making PBAT a very promising biodegradable material for a wide range of potential applications, from medical devices to agricultural and packaging films. However, although PBAT has been recognized as a good quality candidate for BPs, its lower stiffness compared with conventional plastics has limited its use in a wider range of applications.

2.2 | Poly(caprolactone)

PCL is a biodegradable polyester and was first synthesized in the 1930s by ring-opening polymerization of ε-caprolactone. PCL is a semi-crystalline and highly hydrophobic polymer with a melting point of 63°C and a glass-transition temperature of −60°C.[26] It has a tensile strength of 16 MPa and tensile modulus of 0.4 GPa. In addition, PCL has longer degradation times than PLA, which makes it suitable for applications where long degradation times are required.[27,28] Owing to its low melting temperature, PCL is easily processed by conventional melting techniques and can be filled with stiffer materials (particles or fibers) for better mechanical properties. PCL scaffolds have been used for tissue engineering of bone and cartilage.[27,29] Since the homopolymer has a degradation period of 2 years, copolymers have been synthesized

to accelerate the rate of bioabsorption. For example, copolymers of ε-caprolactone with DL-lactide have yielded more flexible materials with higher degradation rates than PCL. The high permeability of PCL to various agents has made it an important candidate for the development of drug delivery systems.

2.3 | Poly(lactic acid)

Poly(lactic acid) or polylactide (PLA) is a thermoplastic aliphatic polyester derived from renewable resources, such as corn starch, tapioca roots, chips or starch, or sugarcane and rice.[30,31] In the year 2010, PLA was the second most important bioplastic of the world made from lactic acid and it is used in the food industry to package sensitive food products. It is not a polyacid (polyelectrolyte), but rather polyester. However, PLA is too fragile and incompatible with many packaging manufacturing processes, hence there is a need to strengthen it with additives. PLA is biocompatible and makes it a perfect candidate for medical implants intended to be absorbed by the body. It is produced by different polymerization routes, namely, ring opening polymerization (ROP), polycondensation and other direct methods (eg, azeotropic dehydration and enzymatic polymerization).[32] ROP method is the preferred method for the production of PLA due to the fabrication of high molecular weight PLA for various applications that is, (eg, packaging, textiles, pharmaceutical products, and biomedical devices).[30–32]

PLA has at least, three stereoisomers, namely: poly(L-lactide) (PLLA), poly(D-lactide), and poly(DL-lactide) (PDLLA), which result from the presence of two chiral carbon centres.[32] In this review, in order to avoid any confusion, PLA will be used to describe all PLA-based polymers. The properties of PLA are influenced by several factors, such as source, the component isomers, the processing routes, and molecular weights. It is mainly affected by stereochemistry and thermal history, which also influence its crystallinity and, therefore, resulting properties. For instance, when PLLA content is higher than 90%, PLA tends to be highly crystalline. However, melting temperature (T_m) and glass-transition temperature (T_g) of PLA decrease with decreasing PLLA content. Table 1 presents the main physical properties of PLA-based polymers.[22,30–33]

PLA possesses remarkable properties, which include biocompatibility, UV stability, clarity, and lustre. The biodegradability and biocompatibility of PLA enabled it to be exploited in various packaging and biomedical applications. However, there are some drawbacks such as slow crystallization, low glass transition and brittleness that hinder the success of PLA.[32,34] A lot of effort has been directed at modifying PLA in order to overcome these drawbacks and match the end-use applications. Several modifications such as blending with other polymers, copolymerizing with functional monomers, aminolysis, and reinforcing with different fillers have been explored as suitable strategies. On the other hand, the use of nanofillers, yielding so-called "nanocomposites materials," merit special attention due to the capability of these particles to enhance mechanical and thermo-mechanical properties as well as to provide additional functionalities at fairly low contents, namely, below 10 wt%.

2.4 | Polyhydroxyalkanoates

Polymers from renewable resources have gained significant attention in recent decades due to environmental issues and the realization of limited petroleum resources. Among the natural polymers, polyhydroxyalkanoates (PHAs) comprise a family of biodegradable polyesters that are produced by an extensive variety of microorganisms for intracellular carbon and energy storage purposes.[35] PHA synthesis is promoted by unbalanced growth during the fermentation and accumulation of PHA granules as part of a survival mechanism of the microbes.[36] For instance, poly(3-hydroxybutyrate) (PHB), poly(3-hydroxyvalerate) (PHV) and their copolymer poly(3-hydroxybutyrate-*co*-3-hydroxyvalerate) (PHBV) are typical examples of short-chain-length PHAs, whereas poly(3-hydroxyoctanoate) (PHO) and poly(3-hydroxynonanoate) (PHN), which are primarily formed as copolymers with 3-hydroxyhexanoate (HHx), 3-hydroxyheptanoate (HH) and/or 3-hydroxydecanoate (HD), are typical examples of MCL-PHAs. More than

TABLE 1 Physical properties of PLA[22,30–33]

Polymer	Elastic modulus (GPa)	Tensile strength (MPa)	Elongation-at-break (%)	T_m (°C)	T_g (°C)
PLA	0.35-3.5	21-60	2.5-6	150-162	45-60
PLLA	2.7-4.14	15.5-150	3.0-10	170-200	55-65
PDLLA	1-3.45	27.6-50	2.0-10.0	-	50-60

Abbreviations: PLA, poly(lactic acid); PLLA, poly(L-lactide); PDLLA, poly(DL-lactide).

150 different PHA monomers have been identified, which renders them the largest group of natural polyesters.[37]

3 | NANOFILLERS

There are numerous nanoparticles that have been used in the production of nanocomposites and are well defined extensively in the literature.[38–40] These nanoparticles are commonly divided into fibers (1D), nanoplatelets (2D), or particles (3D) depending on the number of dimensions they display in the nanoscale.[41] They generally differ from the microparticles commonly used in the composite sectors by a greater surface area. Nanofillers are among the most scientifically investigated materials which are readily and industrially available since they are the target of numerous commercial trials and discussions. The first commercialized nanocomposite was for a piece of car equipment (Toyota) made from nylon-6 clay hybrids.[42,43]

3.1 | Fibers (1D)

One dimension (1D) symbolizes nanomaterials outside the nanoscale. This leads to needle like-shaped nanomaterials which include nanotubes, nanorods, and nanowires. 1D nanomaterials can be amorphous or crystalline, single crystalline or polycrystalline, chemically pure or impure, standalone materials or embedded in within another medium and metallic, ceramic, or polymeric. Highly conductive one-dimensional (1D) metal nanowires such as silver nanowires (AgNWs) can be a good conducting additive in relation to percolation with 1D and carbon nanotubes (CNTs). This can provide the preparation of a mixed solution of a polymer and conducting particles that contain a large amount of conducting material. The one-dimensional shape of the fiber can translate the unique properties of graphene nanocomponents into the macroscopic structure needed for flexible and wearable electronic applications.[44,45]

3.2 | Nanoplatelets (2D)

Two-dimensional (2D) nanomaterials exhibit plate-like shapes and include nanofilms, nanolayers, and nanocoatings. 2D nanomaterials can be amorphous or crystalline, made up of various chemical compositions, used as a single layer or as multilayer structures, deposited on a substrate, integrated into a surrounding matrix material and metallic, ceramic, or polymeric. A typical example of 2D nanomaterial is graphene. Graphene nanoplatelets are the basic building block of 0D fullerene, 1D CNTs, and 3D graphite. It is a single-atomic-thick, two-dimensional (2D) sheet composed of sp^2 hybridized carbon atoms arranged in a honeycomb structure with a carbon-carbon bond length of 0.142 nm. It has a high surface area, gas impermeability, electrical conductivity, thermal conductivity and superior mechanical properties.[46–48] Graphene has a unique planar structure, as well as novel electronic properties, which have attracted huge interest from scientists and showed great potential for improving electrical, mechanical, thermal, and gas barrier properties of polymers.[47,49–51]

3.3 | Particles (3D)

Bulk nanomaterials are materials that are not confined to the nanoscale in any dimension. These materials are thus characterized by having three arbitrarily dimensions above 100 nm. In terms of nanocrystalline structure, bulk nanomaterials can be composed of multiple arrangements of nanosize crystals, most typically in different orientations. With respect to the presence of features at the nanoscale, 3D nanomaterials can contain dispersions of nanoparticles, bundles of nanowires, and nanotubes as well as multinanolayers.[51,52]

4 | SUMMARY OF THE FACTORS AFFECTING THE SELECTIVITY OF THE NANOFILLERS IN POLYMER BLENDS

It is well known that the immiscible polymer blends consist of two phases in which a certain filler can locate, and the localization of the filler determines the final properties of the resultant blend composites.[53–55] There are different factors which have been proposed to have an influence on the preferential localization of the filler in polymer blends.[56–60] The preferred localization of the filler in most blend composites is controlled by thermodynamic factors emanating from polar and interactions between the fillers and the polymer phases. In most studies[56,61] in became very clear that the filler tends to locate in the phase with high affinity during mixing process. The filler localizes in one of the phases in such a way that there is reduction in the interfacial energy. It becomes apparent that the filler prefers a less viscous phase in order to minimize the interfacial energy.

Furthermore, the localization of the filler in an equilibrium may be estimated by Young's equation (Equation 1) through the calculation of the wetting coefficient (ω_a)[62–64] as shown below:

According to the equation, consider two phases that is, polymer 1 and polymer 2

$$\omega_a = \frac{\gamma_{\text{nanofiller}-\text{polymer1}} - \gamma_{\text{nanofiller}-\text{polymer2}}}{\gamma_{\text{polymer1,2}}} \quad (1)$$

The interfacial energy between the filler and polymer 1 is denoted by $\gamma_{\text{nanofiller - polymer1}}$, while the interfacial energy between the filler and polymer 2 is symbolized by $\gamma_{\text{nanofiller - polymer2}}$and the interfacial energy between the two polymer phases is indicated by $\gamma_{\text{polymer1, 2}}$. The interpretation of the wetting coefficient (ω_a) equation is such that, if the wetting coefficient is higher than 1, the filler is anticipated to be located in polymer 2, whereas if the wetting coefficient is lower than −1, the preferred localization of the filler is assumed to be in polymer 1. If the calculated value of the wetting coefficient (ω_a) is found to be between 1 and −1, the preferential localization of the filler is the interface of the two polymers. According to the literature,[61,62,64] the interfacial energy can be calculated from the surface energies as well as the disperse and polar component using both the harmonic mean (Equation (2)) and geometric mean equations (Equation (3)). Haarmonic mean equation is normally used for low energy materials while geometric mean equation is relevant for low-energy and high-energy materials.

$$\gamma_{12} = \gamma_1 + \gamma_2 - 4\left(\frac{\gamma_1^d \gamma_2^d}{\gamma_1^d + \gamma_2^d} + \frac{\gamma_1^p \gamma_1^p}{\gamma_1^p + \gamma_2^p}\right) \quad (2)$$

$$\gamma_{12} = \gamma_1 + \gamma_2 - 2\left(\sqrt{\gamma_1^d \gamma_2^d} + \sqrt{\gamma_1^p \gamma_2^p}\right) \quad (3)$$

From the equations, γ_1, γ_2 represent the surface tensions of phase 1 and 2, while γ_1^d and γ_2^d denotes the dispersive section of the surface tensions of phase 1 and 2, respectively, while γ_1^p and γ_2^p represents the polar fractions of the surface tension of phase 1 and 2, respectively.

Besides the thermodynamic effect on the preferential localization of the filler in a polymer blend, kinetic effects such as (a) compounding sequence, (b) melt viscosity, (c) melt compounding time, and (d) shear rate play a vital role on the localization of the filler.[60–62] It is worth mentioning that the kinetic factors are important if one is to selectively control the filler localization between two polymer phases. The principle of compounding sequence for control localization is such that there is a successive mixing, whereby the filler is premixed with phase component that it has less affinity with, and then mixed with the second component in the second step of mixing. The approach is based on filler particles migrating from the non-interacting phase towards more interacting component. For an example, Bai and co-workers[61] kinetically controlled graphene localization in a co-continuous polymer blends via melt compounding. In their study, the authors mentioned that the graphene (GNPs) filler preferred to be localized in the polystyrene phase than PLA phase. During preparation, GNPs were premixed with non-interact PLA phase before mixing with the interact PS. The method resulted in trapping of GNPs at the interface during melt nixing process. In polymer blends, melt-viscosity play a significant role in affecting the final filler localization and the final morphology of the blend composites at large. In a polymer blend composites, a polymer with less viscosity seems to have a better wetting coefficient, as a result it becomes easy for the nanoparticles/filler to diffuse into it. It is also apparent that if the processing conditions are controlled, fillers can be selectively localize at the interface, co-continuous region or within the two phases. Furthermore, it became clear that the different mixing times play a huge role as to where the nanofiller may be localized. Huang et al[57] showed that different mixing times resulted in different localization (viz., PLA phase, PCL phase and/or interface) for CNTs in PLA/PCL blend. Mixing time in this study was explained as the time after incorporating PCL into the premixed PLA/MWCNTs composite. The authors observed a migration of MWCNTs to the phase boundaries and some prevail in the PLA phase after 1 minute of mixing. However, with increase in time from 1 minute to 4 minutes, there was an accumulation of the MWCNTs at the interface. Furthermore, an increase in time up to 20 minutes saw most of the MWCNTs dispersing into the PCL phase. According to the observation of the results obtained, it became very clear that more mixing time is required for nanofillers to migrate from one phase to another. It is very interesting to note that with a careful control of mixing parameters and process, specific localization of the filler may be attained by kinetic aspects.

5 | MORPHOLOGY AND NANOFILLER LOCALIZATION IN THE BP BLENDS

The properties of the BP blends can be improved through the addition of the nanofillers to achieve a blend nanocomposite. The control of filler localization, its distribution, adhesion between the two polymers and nanofiller(s) play an important role in controlling the final properties of the blend composite. Generally, the addition of nanofiller does not only improve the reinforcement of BP blends, but also improves the interfacial adhesion between the two polyesters. It is well documented in the

literature that the properties of nanofillers(s) filled BP blends depends on the arrangement of the nanofillers in the polymer. The addition of the nanofiller(s) into a polymer blend may result in localization of the nanofiller within different polymeric phases, specific polymeric phases and/or at the interphase. The preferred localization of the nanofillers into BP blend is mainly driven by thermodynamic (viz., enthalpic interaction between each polymer and nanoparticles) and kinetic factors (ie, viscosity ratios of the two polymers).[65] It is expected that the melt mixing of two polymers with different molar mass and viscosity with nanofillers would give rise to the selective localization of the filler. Sivanjineyulu et al[66] investigated the selective localization of CNTs and organoclay in biodegradable poly(butylene succinate)/polylactide blend-based nanocomposites. In the hybrid filler-composites, the CNTs were found in the continuous PBS matrix, while the organoclay settled in the PLA phase. The preferential localization of organoclay in the PLA domains was ascribed to the interactions between PLA and the organically modified surface of clay. However, the authors did not provide a reason for the localization of CNTs in the continuous PBS matrix. The preferential localization of CNTs in the PBS matrix as opposed to the PLA phase can be attributed to the low viscosity of PBS during processing. In the study conducted by Wokadala et al,[65] the clays in all samples were mainly found in the butylated starch phase as opposed to the PLA phase with the exception of C20A clay (Figure 1). Two possible reasons were given by the authors in relation to the preferential location of the clay in butylated starch phase. Firstly, it was recognized that the clays are not completely hydrophobic; there were high chances that the interfacial tensions were higher in PLA in contrast with butylated starch, resulting in the preferential location of clays within the starch phase in most composites. Secondly, the location of the clay nanofillers in the starch phase could be due to the difference in the viscosity ratio between the butylated starch phase and the PLA phase. It is well known that the viscosity ratio between two polymers affects the level of mixing. The clay nanofillers would preferentially locate in the starch phase due to lower viscosity when compared to PLA phase. Mofokeng and Luyt[67] investigated the morphology and thermal degradation of melt-mixed poly(hydroxybutyrate-co-valerate) (PHBV)/PCL/TiO_2 polymer blend nanocomposites. In their study, the authors reported that the TiO_2 nanoparticles were present in both phases of the blend and the interface between PHBV and PCL. One would expect the nanoparticles to locate in the PCL phase because PHBV had higher molar mass and degree of crystallinity, but lower melt flow index, that is, higher viscosity. Similar surface energies, dispersive, and polar parts of PCL and PHBV are the main reasons for no selective location at any of the two polymers. The calculation of the interfacial tension (Young's equation) was used to establish the localization of the zinc oxide (ZnO) into the PLA/PCL BP blend.[68] The content of ZnO added into the BP blend was varied between 2% and 6%. According to the authors, if the wetting coefficient (ω_{12}) is $\omega_{12} > 1$, ZnO nanoparticles are expected to be located into the PLA phase. If the wetting coefficient $\omega_{12} < -1$, ZnO is anticipated to be located in the PCL phase. Furthermore, if the wetting coefficient is between $-1 \leq \omega_{12} \leq 1$, ZnO nanoparticles are expected to be at the interface. The authors recorded a wetting coefficient value of 2.09, meaning that the ZnO nanoparticles were located in the PLA phase. It became apparent in some cases that, in order to improve the dispersion or compatibility of nanofillers into BP blends, functional groups are supposed to be doped into nanofillers. The introduction of nitrogen (N) as a functional group into graphene to improve its dispersion when incorporated into poly (butylene succinate)/polylactide blends was investigated by Wu et al.[69] The fabricated nanofiller in the form of nitrogen-doped graphene (NG) is believed to have polar oxygen and nitrogen as well as large aspect ratio to improve its interaction with BPs. Different contents of NG (0, 0.3, 0.5, and 1 wt%) were incorporated into a fixed PBS/PLA (70/30) blend. The blend nanocomposites were prepared by melt compounding. Graphene functionalized with nitrogen reduced the particle size of the minor phase that may be ascribed to the compatibility of graphene for BP blend. Moreover, graphene was selectively localized in the PBS matrix while some graphene particles were found at the interface and prevented coalescence of PLA droplets. To improve certain properties of BP/nanofiller blend nanocomposites, filler localization had to be controlled. The selective localization of graphene (GE) at the interface of a PCL/PLA blend was studied by Huang and co-workers.[70] The composites and blend composites were prepared by three different steps/methods (i) solution mixing, compression molding, and followed by adsorption-desorption method. The adsorption-desorption method was employed in order to confine the graphene (GE) at the interface of the PCL/PLA blend. The GE sheets were found to be located at the interface of the BP blend and PCL phase. Table 2 summarizes selective studies on the localization and morphology of the nanofiller(s) into BP blends.

6 | MECHANICAL RESPONSES OF BP BLENDS NANOCOMPOSITES

The presence of a filler in its nano-scale dimension in the BP-based blends shows a noticeable impact on the mechanical properties of the resultant BP blend

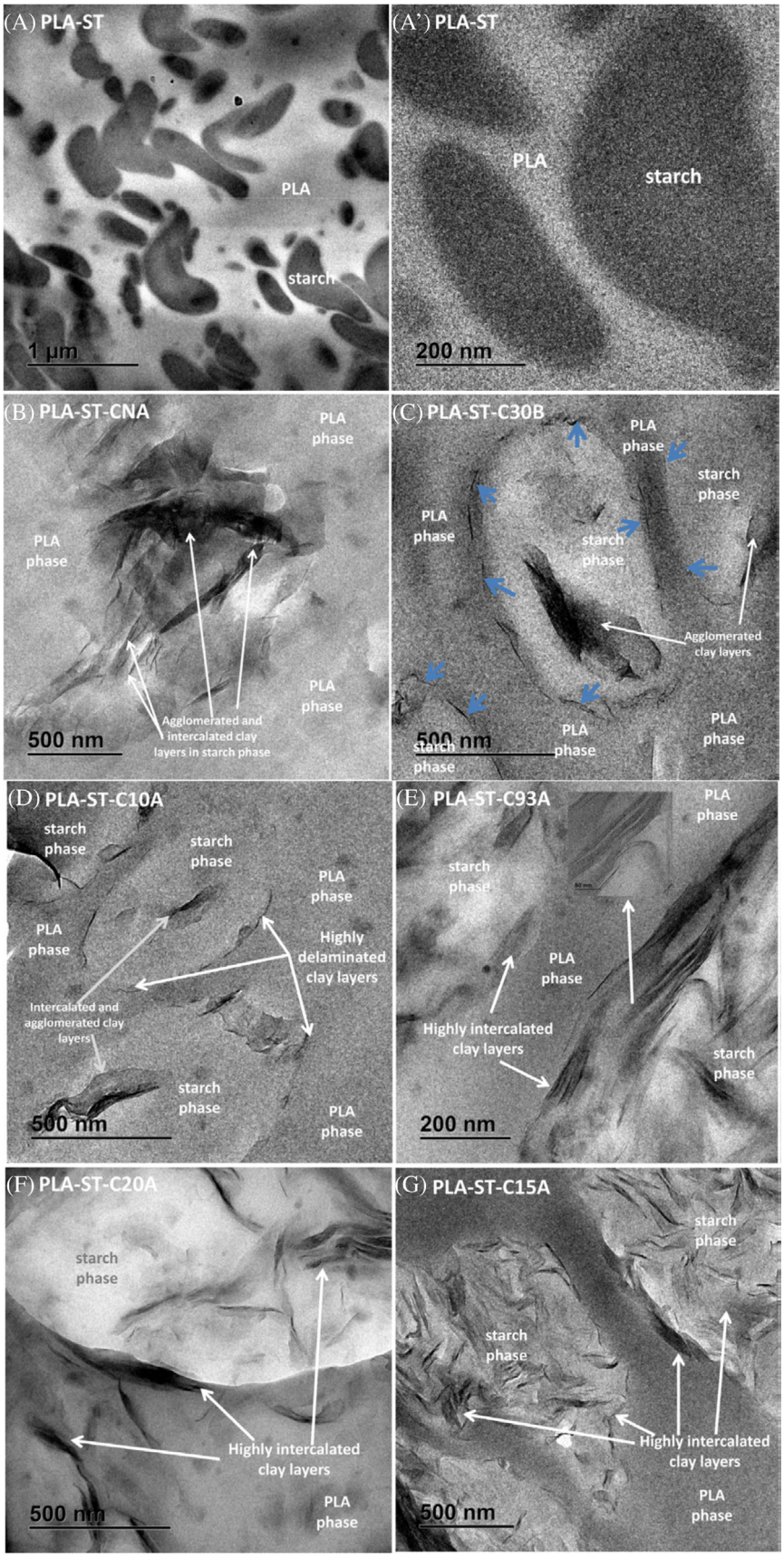

FIGURE 1 Right field transmission electron microscopy (TEM) images of A, A', PLA-ST blend at two different magnifications; B, PLA-ST-CNA; and C, PLA-ST-C0B composites. Arrows indicating the dispersion of silicate layers at different phases and at the interphase. Bright field TEM images of D, PLA-ST-C10A; E, PLA-ST-C93A; and F, PLA-ST-C20A and G, PLA-ST-C15A composites. Arrows indicating the dispersion of silicate layers at different phases and at the interphase.[65] Copyrights Elsevier [Color figure can be viewed at wileyonlinelibrary.com]

TABLE 2 Selective studies on the localization and morphology of the nanofillers into biopolymer blends

Biopolymer blend composite	Processing method	Morphology and nanofiller localization	Refs
Poly(lactic acid)/polybutylene succinate/ graphene oxide **(PLLA/PBS/GO)** (*synthetic-synthetic*)	Melt blending	Scanning and transmission electron microscopy (TEM) showed micron-sized droplets of PBS in the PLLA matrix with the GO found in the PBS.	71
(Poly(lactic acid)/poly(hydroxybutyrate-co-hydroxyvalerate), poly(hydroxybutyrate-co-hydroxyvalerate)/poly(caprolactone), poly(lactic acid)/poly(caprolactone))/ titanium (IV) oxide **(PLA/PHBV/, PHBV/PCL, PLA/PCL)/ TiO_2** (*synthetic-synthetic*)	Melt-mixing using a Brabender Plastograph	TiO_2 in both systems (PLA/PHBV) were dispersed in the PLA phase and interface over PHBV as well as PCL. Furthermore, For PHBV/PCL system, the titania nanoparticles are more dominant in the PHBV phase and the interface.	72
Poly(lactic acid)/poly(caprolactone)/ titanium (IV) oxide **(PLA/PCL/TiO_2)** (*synthetic-synthetic*)	Melt-mixing using a Brabender Plastograph	TEM image of the 25/75 w/w PLA/PCL showed large spheres of one polymer in a matrix of the other phase and the titania nanoparticles were dispersed into the spheres. The nanoparticles were confined to the spheres phase (PLA matrix) because PLA formed spheres in the PCL matrix based on PLA:PCL ratio.	73
Poly(3-hydroxybutyrate-co-3-hydroxyvalerate)/poly(lactic acid)/ sepiolite **(PHBV/PLA/SEP)** (*synthetic-synthetic*)	Samples were prepared by twin-screw co-rotating extruder	According SEM image, the sepiolite nanofibers were selective located in the PHBV phase.	74
Poly(3-hydroxybutyrate-*co*-3-hydroxyvalerate)/poly(lactic acid)/ sepiolite and cloisite 30B **PHBV/PLA/(SP and C30B)** (*synthetic-synthetic*)	Samples were fabricated by an internal mixer	There was no mentioning of the preferential location of the nanofillers. A good degree of dispersion of CB 30 and Sepiolite in the PHBV/PLA was obtained and furthermore, no aggregates were found.	75
Poly(lactic acid)/poly(caprolactone)/graphite nanoplatelets **PLA/PCL/GNP** (*synthetic-synthetic*)	Melt-mixed by Brabender Plasti-corder	Electron microscopy showed that the nanoplatelets were dominant in the PCL phase.	76
Poly(lactic acid)/poly(caprolactone)/ functionalized thermally exfoliated reduced graphene oxide **PLA/PCL/(f-TERGO)** (*synthetic-synthetic*)	The investigated samples were produced by melt-mixing in a HAAKE PolyLab OS Rheomix mixer	TEM and POM micrographs showed that the f-TERGO nanoparticles were mostly located in the PCL phase as a result leading to a high melt-viscosity ratio.	77

nanocomposites. In modern communities, mechanical properties of the BP blend nanocomposites account for their enormous utility in various essential applications such as food packaging, biomedical facilities, and motor industries.[78,79] Nonetheless, an overall mechanical response of the BP blend nanocomposites is affected by several factors including localization and dispersion of the nanofiller, which are influenced by the preparation methods, thermodynamic and kinetic factors. The localization of the nanofiller within the BP blends is dependent on the physicochemical properties of entities of the blends which entail, inter alia, crystallinity, polarity, viscosity, hydrophobicity or hydrophilicity, affinity, and degree of porosity.[80–82] These attributes of the individual BP materials determine an ultimate localization of the nanofiller in which, depending on the type of

morphological aspects, could either be at the interphase, discontinuous phase or continuous phase in the heterogeneous systems. However in the homogeneous systems, the nanofiller particles would disperse uniformly or as clusters across the co-continuous phases of the components of the BP blends. For example, Urquijo and coworkers[83] investigated the effect of localization of CNTs on the mechanical properties of the almost co-continuous morphology of the resultant 60/40 PLA/-PBAT BP blend prepared by melt mixing method. It was discovered that the impact strength increased by 2.5 folds for 60/40/3 PLA/PBAT/CNT nanocomposite with respect to pristine 60/40 PLA/PBAT blend, due to the location of CNTs in the minor PBAT phase which enables an effective stress transfer mechanism for the entire nanocomposites. Nevertheless, BPs are categorized into natural and synthetic biomaterials, thus their mechanical properties vary interestingly. However, the process of blending natural and synthetic biomaterials may result in excellent mechanical response which exceeds that of the respective individual BPs of the BP blend.[79,84,85] Furthermore, the treatment of the nano-filler and/or individual BP materials for surface modification prior to the preparation of the BP blend nanocomposites amounts to significant enhancement of the mechanical properties of the resultant BP blend nanocomposites which are essential for food packaging. In the work of Sessini and coworkers,[86] the cellulose nanocrystals (CNCs) were stabilized against thermal strain using 1.0% basic buffer solution of sodium hydroxide followed by the "grafting from" technique to afford the CNC-g-PCL and CNC-g-PLLA BP nanocomposites at the 1 wt% concentration of CNCs, respectively, via the ring open polymerization method. Extrusion process and a subsequent compression molding were utilized to prepare a pure 70/30 PLA/PCL BP blend which is denoted by M70PLA and BP blend nanocomposites designated with M70PLA/CNC, M70PLA/CNC-g-PCL, and M70PLA/CNC-g-PLLA, respectively. For all prepared BP blend nanocomposites, the reported mechanical properties such as elastic modulus and tensile strength increased noticeably (Figure 2) due to the localization of the CNCs at the interphase of the individual PLA and PCL BP materials. However, the elongation at break of M70PLA/CNC and M70PLA/CNC-g-PCL showed a drastic diminish suggesting that the good compatibilization was realized when blending the pristine blend with M70PLA/CNC-g-PLLA due to an outstanding interfacial adhesion of CNCs and PLLA matrix. It is clear from the work of Sessini et al.[86] that in all

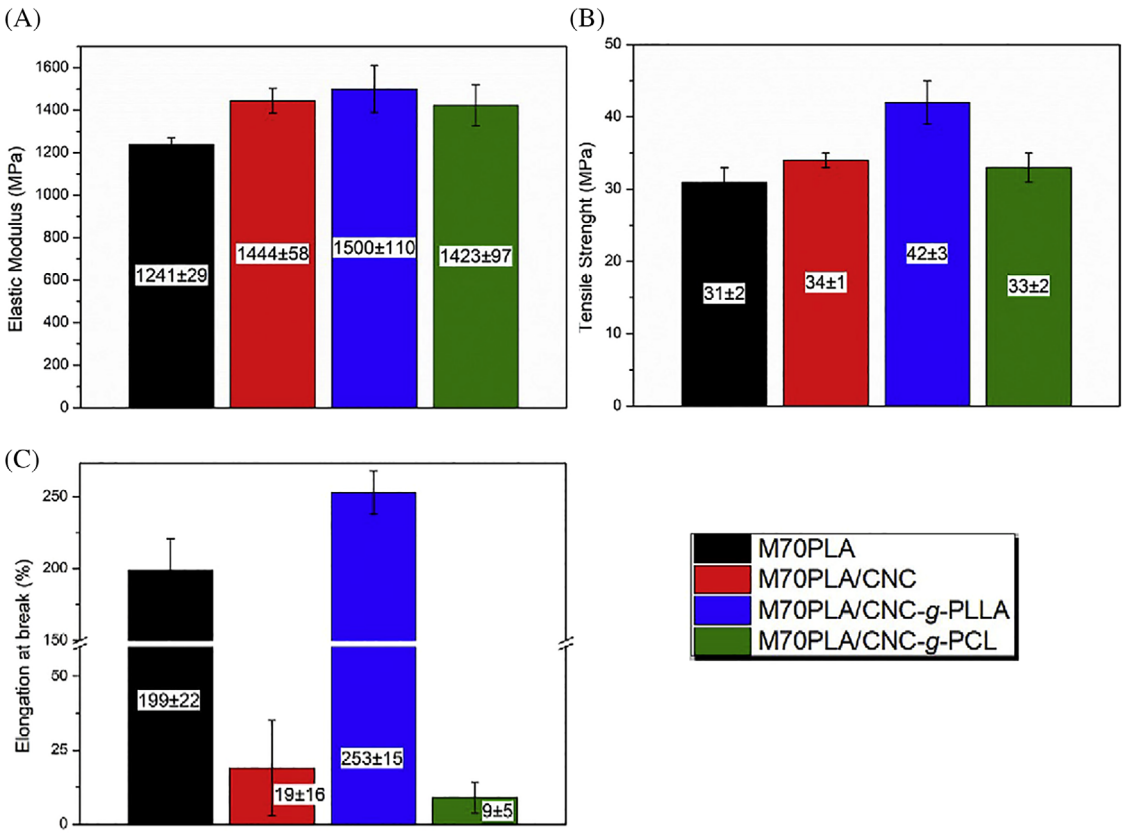

FIGURE 2 Mechanical properties of PLA/PCL blend and the CNC-based nanocomposites.[86] Copyrights Elsevier. CNC, cellulose nanocrystal; PCL, poly(caprolactone); PLA, poly(lactic acid) [Color figure can be viewed at wileyonlinelibrary.com]

treatments, CNC was either localized in the PCL phase or at the interphase of PCL and PLA. An interesting thing to achieve would be manipulating the localization of CNC in all phases of the PLA/PCL blend and investigate the mechanical properties of the resulting blend composites. We propose two approaches; The first approach involves simultaneously adding a mixture of CNC-g-PCL and CNC-g-PLLA to the M70PLA. The second approach involves simultaneous grafting of PLLA and PCL chains onto CNC to form PCL-CNC-g-PLLA and incorporate it to the M70PLA. Infact, the latter approach is cost effective than the former because it involves one step grafting.

In general, the incorporation of nano-filler into a combined system of synthetic BP and natural BP has shown a phenomenal improvement of the mechanical properties of the resultant BP blend nanocomposites. A variety of natural biopolymeric materials such as, among others, alginate, cellulose, starch, chitosan and lignin are generally extracted from plants, vegetables and fruits whereas gelatin, proteins and nucleotides are found in living creatures.[87–91] Quite interesting discoveries were established on the manipulation of mechanical properties emanating from the introduction of nanofillers into the natural-synthetic BP hybrid blends. Mathew and coworkers[92] reported the influence of montmorillonite (Mt) and silver nanoparticles (AgNPs) derived from the *in situ* generation with polymer matrix on the mechanical properties of polyvinyl alcohol/boiled rice starch nanocomposites. The results showed a marked increase of the tensile strength and Young's modulus of PVA when either boiled rice or a mixture of boiled rice and Mt were added. The authors attributed their results to the formation of intermolecular bonds between PVA and starch, and strong intermolecular interaction between Mt, PVA and boiled rice starch.

However, the addition of the AgNPs to form PVA/Mt/AgNP/boiled rice composite slightly decreased the tensile strength and Young's modulus by 8.4% and 38.3%, respectively, when compared with the PVA/Mt/boiled rice composite. Moreover, elongation at break manifested a general decrease with the introduction of nanoparticles to the PVA/boiled rice starch hybrid blend, and this trend was associated with the rigidity of the nanofillers that resulted in the immobility of polymer chains, hence the decrease in ductility of the nanocomposites. In another study reported by Rukmanikrishnan and coworkers,[93] the effect of titanium oxide (TiO_2) on the mechanical properties of ternary blend consisting of natural k-Carrageenan (k-C), xanthan gum (X) and gellan gum (G) BP materials at the constant ratio of 6:2:1, prepared by solution casting method was investigated. The tensile strength and tensile modulus showed an increasing trend with the increase of the TiO_2 nanoparticles reaching the highest values of 56.1 $\pm$ 1.90 MPa and 6.2 $\pm$ 0.17 GPa at 7-wt% TiO_2, respectively. On contrary, the decrease in elongation at break of the k-C/X/G/TiO_2 nanocomposites with the increase of TiO_2 content was ascribed to the poor dispersion of the hydrophobic TiO_2 nanoparticles within the ternary blend. In recent years, a plethora of BP blends composed of natural and/or synthetic bio-macromolecules is utilized as polymer matrices wherein the nanofillers can be incorporated to afford disparate natural-natural, natural-synthetic or synthetic-synthetic BP blend nanocomposites with improved mechanical properties has been the subject of research investigation. Table 3 collates the different mechanical properties observed on various BP blend nanocomposite systems prepared using dissimilar preparatory methods:

7 | THERMAL BEHAVIOR OF BP BLEND NANOCOMPOSITES

Viable analyses of the degree of miscibility for the BP blend nanocomposites, apart from visual microscopic techniques, are accurately deduced from the thermal properties affected by thermal characterizations such as differential scanning calorimetry (DSC) and thermal gravimetric analysis as well as dynamic mechanical analysis. The thermal behavior of the BP blend nanocomposites is regarded as one of the indispensable aspects for the applicability of nanocomposites in various fields including nanotechnology, food packaging, and paper industries.[105] The extent to which the BP materials interact in the blend affects the ultimate thermal properties of the resultant BP blend nanocomposites. Furthermore, the preparation methods and treatment of the components of BP blend nanocomposites would inevitably influence the thermal behavior and the extent of intermolecular interaction of the entities of the envisaged BP blend nanocomposites. Furthermore, it is generally known that the addition of a filler into any polymer blend may improve/enhance crystallization of both polymers or one polymer.[106] More importantly, the localization of the nano-filler and its distribution in the BP blend regulates the interfacial adhesion and controls the mobility of polymer chains which in turn result in changes of thermal behavior in comparison with the pristine BPs. The melting temperatures of the respective crystalline or semi-crystalline BP materials determine the degree of miscibility amid the BP components.[94] In contrast, the glass-transition temperature (T_g) imparts the mobility of chains of the BPs within the amorphous region, and it is affected by the presence of nano-filler particles. Tian and coworkers[107] reported the change of T_g for the natural-

TABLE 3 Summarized studies on the mechanical properties of biopolymer blends/nanofillers

Biopolymer blend systems	Processing methods	Mechanical properties	Refs
Polylactic acid/chitosan/zinc oxide (**PLA/CS/ZnO NPs**) (*natural-synthetic*)	Solution casting	The incorporation of ZnO NPs into the PLA/CS blends significantly increased the tensile strength of the composites by 34%-45% up to 2 wt% of ZnO NPs loading. But, the tensile strength of the composite declined when the amount of ZnO NPs increased up to 3 wt%.	94
Poly(lactic acid)/lignin/silver nanoparticles **(PLA/lignin/AgNPs)** (*natural-synthetic*)	Solution casting	The tensile strength (TS) of the neat PLA film was 38.6 ± 9.2 MPa, which was increased to 43.4 ± 8.0 MPa after blending with lignin. The increased TS of PLA/lignin film might be due to high compatibility between lignin and PLA biopolymer. The TS of the PLA-based films increased further up to 45.5-45.4 MPa when AgNPs were incorporated.	95
Polylactic acid/poly(caprolactone)/ hydroxyapatite **(PLA/PCL/nHA)** (*synthetic-synthetic)*	Melt blending	The addition of nHA produced an increase of the Young modulus, while the tensile strength remains quite constant for all investigated nanocomposites.	96
Poly(lactic acid)/silica rubber -atactic poly (D-lactic acid) **(PLLA/SiO_2-r-PDLA)** (*synthetic-synthetic)*	Solution blending and injection molding	The tensile strength and modulus are somehow maintained, probably due to twin effects of rigid silica particles and stereo complex crystallites formation. As a result, strain at break and tensile toughness are tremendously enhanced with the addition of SiO_2-r-PDLA nanofillers.	97
Epoxy functionalized graphene-poly(lactic acid)/butylenes-adipate-co-terephthalate and cloisite 15A-poly(lactic acid0/ butylenes adipate-co-terephthalate **(EFG-PLA/PBAT and C15A-PLA/PBAT)** (*synthetic-synthetic)*	Melt/physical mixing	Addition of 5 wt% of EFG in the PLA/PBAT blend showed an improved elastic modulus and the elongation at break. This increase of mechanical properties of nanofillers-PLA/PBAT blends can be due to the better dispersion of C15A in the PLA phase. For the EFG-PLA/PBAT blend, the possible presence of EFG in the PBAT phase favoured the interactions between the epoxy function of graphene and the carbonyl groups of PBAT leading to improved mechanical properties of PLA/PBAT blends.	98
Chitosan/polyvinyl alcohol/Zinc sulfide **(CH/PVA/ZnS)** (*natural-synthetic*)	Solution casting	The tensile strength of chitosan/PVA increases with the increase of the content of ZnS in all nanocomposites despite the treatment of the blend with different plasticizers (grade glycerol (G), citric acid (C), ascorbic acid (AS). Nanocomposite treated with AS revealed better enhancement than the ones treated with G and C due to the presence of hydroxyl, ketone and ether functional groups. However, the elongation at break shows a decreasing trend for all nanocomposite samples. The improvement of the tensile strength was due to the molecular interaction which takes place between the chitosan, PVA and ZnS.	99
Multiwalled carbon nanotube/gelatin/ chitosan (*natural-natural*)	Solution casting	All investigated mechanical properties, tensile strength, elongation at break and tensile modulus increased with the incorporation of MWCNT reaching the highest values of 55 MPa, 1.8% and 335 MPa at 1 wt% of MWCNT, respectively. The ultimate response of the mechanical properties for MWCNT/gelatin/chitosan nanocomposites was ascribed to the tunneling effect emanating from the MWCNT particles.	100

(Continues)

TABLE 3 (Continued)

Biopolymer blend systems	Processing methods	Mechanical properties	Refs
Poly(lactic acid)/Poly(ethylene oxide)/ carbon nanotubes **PLA/PEO/CNT** (*synthetic-synthetic)*	Solution casting	The results showed that the difference stress (N_1) as a function of shear rate increases noticeably with the addition of nanoparticles. The increase of N_1 in the presence of CNT is associated with the orientation of nanoparticles in the flow direction and appropriate interaction between polymer-filler within the PLA/PEO/CNT nanocomposites.	101
Sodium alginate/polyvinyl alcohol/graphene oxide **(SA/PVA/GO)** (*natural-synthetic*)	Solution casting	The tensile strength and Young's modulus of increased from 1.03 ± 0.15 to 1.91 ± 0.10 MPa, and from 1.21 ± 0.20 to 2.92 ± 0.11 MPa from the pristine blend to the addition of GO 2 wt%, respectively. The presence of GO in the sodium alginate/PVA blend diminishes the elongation at break because GO acts as crosslinking agent which result in a decrease of molecular chains in SA and PVA in the nanocomposites.	102
Chitosan/sericin/silver NPs **(CH/sericin/AgNPs)** (*natural-natural*)	Solution casting	All prepared biopolymer blend nanocomposites exhibited a lower tensile strength and an increased elongation at break due to the amorphous nature and a high brittleness of sericin. However, the obtained tensile strength was reported to be sufficient for the application in the wound healing process.	103
Chitosan/Trigonella foenum graecum seed polysaccharide/nano hydroxyapatite **(CH/TFSP/nHA)** (*natural-natural*)	Co-precipitation	Biomimetic nanocomposites comprising nano-hydroxyapatite (nHA), chitosan (CH) and trigonella foenum graecum seed polysaccharide (TFSP), nHA-CH-TFSP, revealed a compressive strength and compressive modulus of 6.7 ± 0.24 MPa and 100 ± 1.4 MPa, respectively, these values fall into the range of cancellous bone. The resulting biomimetic behavior of the biopolymer blend nanocomposites is associated with the intermolecular hydrogen bonding existing between the entities, viable porosity of the nanocomposites and good distribution of nHA nanoparticles within the biopolymer blend.	104

synthetic system, polyvinyl alcohol/corn starch when montmorillonite (MMT) is incorporated to produce nanocomposites prepared by melt compounding. Their results showed one peak at 102°C corresponding to the T_g of PVA/corn starch/MMT nanocomposites indicating good compatibility between PVA and starch due to hydrogen bonding resulting from the hydroxyl groups of PVA. The increase of MMT content enhanced the T_g of the nanocomposites due to the restriction of molecular chains of starch and PVA at the interface on the account of good dispersion as a result of high aspect ratio and reactive surface. The blending of different BPs and the introduction of nano-filler could enhance the thermal stability through which the protection of the resultant BP blend nanocomposites against heat can be attained. For example, Sebastián Bonardd and coworkers[108] conducted an investigation on the thermal stability of poly(ethylene oxide) (PEO)/chitosan blend and PEO/chitosan blend nanocomposites and obtained different thermal behaviors on the addition of gold nano-particles. The authors reported that the thermal stability of PEO reduced with the addition of gold nano-particles (AuNPs) (Figure 3) due to poor interaction between PEO and AuNPs thus PEO become labile and degraded earlier through the scission of its backbone. Whereas, chitosan manifested an observable increase in thermal stability in the presence of AuNPs due to the good molecular interaction between the components leading to adsorption of AuNPs on to chitosan causing inhibition of rapid degradation process as shown in **(**Figure 3**)**.

In recent years, the preparation of BP blend nanocomposites has been a subject of great interest in

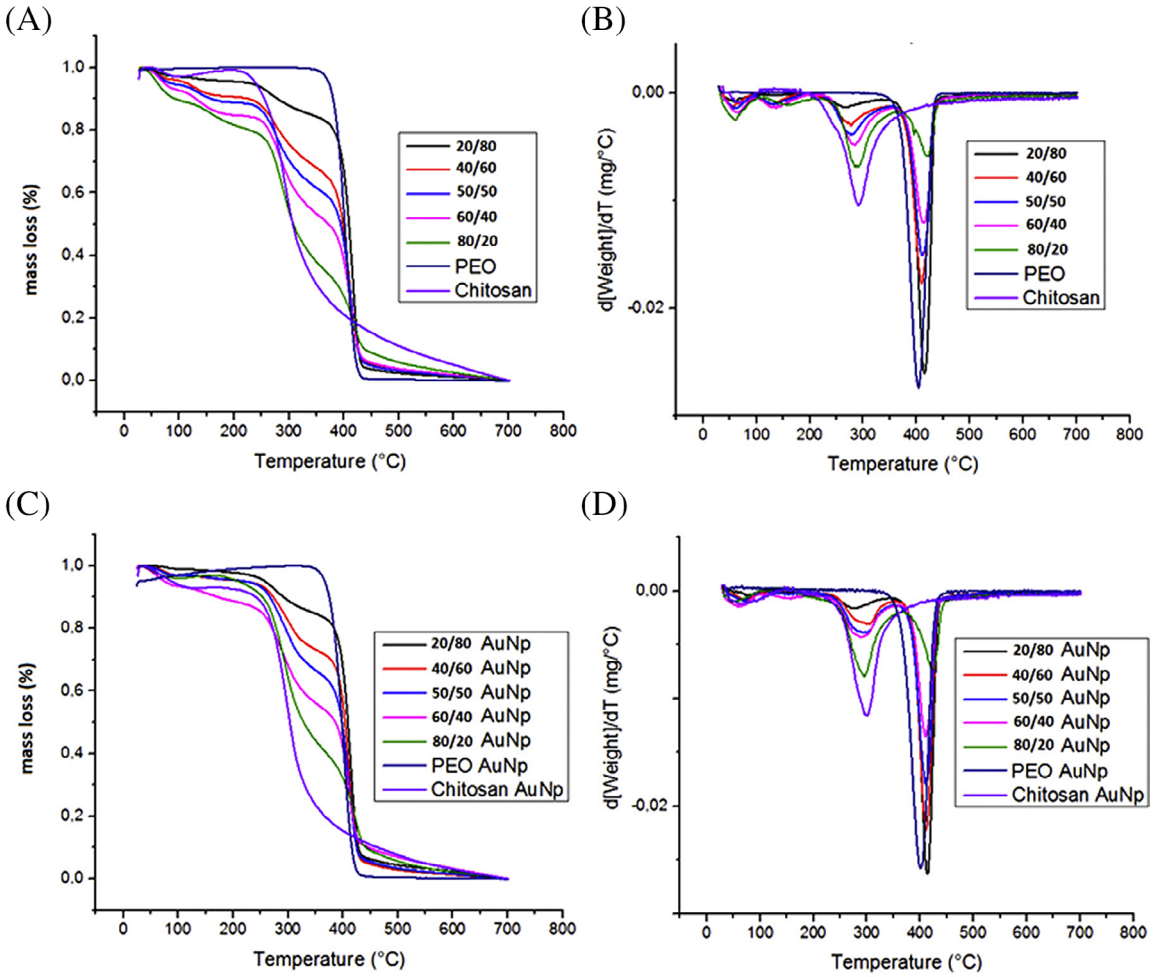

FIGURE 3 Degradation (thermogravimetric analysis [TGA], left) and differential thermogravimetric analysis (DTGA, right) curves for CS/poly(ethylene oxide) (PEO) blends, A, without and, B, with gold nanoparticles for each biopolymers and biopolymer blend/AuNPs nanocomposites.[108] Copyrights Elsevier [Color figure can be viewed at wileyonlinelibrary.com]

both academia and industry. The effect of treatment of either one, or/and all components of the BP blend nanocomposites prior blending or incorporation of the nano-filler on the thermal behavior was also investigated. Generally, natural BP composed of large amorphous portion when compared to most synthetic BPs that constitute predominantly crystalline region according to the analyses conducted by the DSC. The thermal stability of various BP blends can be significantly improved by the addition of the nano-particles that adsorb on the BP surface due to good interaction which is essential to the enhancement of the thermal stability. Also, the localization of the nano-filler and its dispersion influence the thermal stability of the resultant BP blend nanocomposites. Many investigations were done on different compositions of BP blends and the influence of incorporating nanofillers in order to achieve the envisaged thermal properties of the BP blend nanocomposites. Table 4 summarizes the recent literature data of a variety of BP blend nanocomposites and their observed different thermal behaviors.

8 | ELECTRICAL AND THERMAL CONDUCTIVITY OF BP BLEND NANOCOMPOSITES

The addition of conductive nanofiller in BP blend provides great potential in the preparation of (semi) conductive products without affecting other properties. It is well known that the thermal and electrical conductivity of a composite and /or blend composite depend on the filler content and filler network behavior. The filler dispersion within the polymer and/or polymer blend is very important to obtain the desired thermal and electrical conductivity values. Few studies[66,70,112] reported on the thermal conductivity and electrical conductivity of BP blend/nanofiller(s) blend nanocomposites. In most cases, the

TABLE 4 Summarized studies on the thermal properties of biopolymer blends/nanofillers

Biopolymer blend systems	Processing methods	Thermal properties	Refs
Poly(lactic acid)-acetyl tributyl citrate/cellulose nanocrystals PLA-ATBC/ Cellulose nanocrystals *(synthetic-synthetic)*	Electrospinning	DSC curve shows an exothermic peak in PLA-PHB-ATBC mat, suggesting that during the heating in DSC analysis ATBC increased the ability of PLA-PHB to crystallize, probably due to the fact that rapid solvent evaporation during the electrospinning process led to quenching conditions and to the formation of disordered crystals. Plasticizer also produced a reduction of about 25°C in the cold crystallization temperature of PLA-PHB due to an increase in the polymers chain mobility.	109
Poly(lactic acid)/poly(caprolactone)/graphene oxide **PLA/PCL/GO** *(synthetic-synthetic)*	Solution and electrospinning method	The addition of GO nanosheets served as nucleating agents for the crystallization of both PLA and PCL phases. The melting peak area and the degree of crystallization of PCL, decreased when the weight fraction of PCL was at 50% and 70%. While for the PLA phase, the variation showed an exact reverse in crystallization at different weight ratios.	110
(Poly(lactic acid)/poly(hydroxybutyrate-co-hydroxyvalerate), poly(hydroxybutyrate-co-hydroxyvalerate)/poly(caprolactone), poly(lactic acid)/poly(caprolactone))/ titanium(IV) oxide **(PLA/PHBV, PHBV/PCL, PLA/PCL)/TiO_2** *(synthetic - synthetic)*	Melt blending	The DSC results confirm that the transition at about 60°C is a glass transition, while the irreversible cold crystallization of PLA is seen as two processes in the step-scan results, one at a lower temperature and the other after the onset of melting of the sample. The three overlapping endotherms around 140-160°C are therefore due to the melting of the cold crystallized PLA and that of the melting and re-melting of PHBV. The glass transition peak in the tan d curve of neat PLA is very intense, with an obvious cold crystallization peak around 100°C, which clearly indicates that in the unblended and unfilled PLA there is a large extent of molecular motion on going from the glassy to the rubbery phase.	72
Natureplast PBE 003/butylene adipate-co-terephthalate/ expanded organoclay **(PBE/PBAT/EOC)** *(synthetic - synthetic)*	Melt compounding	Addition of expanded organo nanoclay at 2 wt% increased the crystallinity of the nanocomposites. However, a farther increase of EOC to 15 wt% diminishes the crystallinity, melting and crystallization temperatures. It was reported that the presence of stearic acid (SA) in the blend composites would have acted as the plasticizer leading to the decrease of T_m, T_c, and crystallinity.	111
Epoxy functionalized graphene-poly(lactic acid)/butylenes-adipate-co-terephthalate and Cloisite 15A-poly(lactic acid)/butylenes adipate-co-terephthalate **(EFG-PLA/PBAT and C15A-PLA/PBAT)** *(synthetic-synthetic)*	Melt/physical mixing	Thermograms of all ternary blends exhibited high thermal stability than the PLA/PCL neat blend. In the case of OMt-PLA/PCL nanocomposites, the onset temperature shifts to the high values compared to the virgin blend. This is habitually attributed to the dispersion state of organomontmorillonite layers in the polymer matrix forming exfoliated and/or intercalated nanocomposites.	98

TABLE 4 (Continued)

Biopolymer blend systems	Processing methods	Thermal properties	Refs
Agar-carboxymethyl cellulose/silver modified montmorillonite **Agar-CMC/Ag-MMT** (*natural-synthetic*)	Solution casting	The thermal stability shows an increasing trend of decomposition from 203.1 to 212.7, 225.0, 229.2 and 245.6°C with the addition of 2, 4, 6 and 8 wt% AgMMT, respectively. It was suggested that the thermal stability increases due to the presence of alumina and silicate layers in the AgMMT nanoparticles which act as the heat insulator by inhibiting the diffusion of volatile product polymer matrix, hence the deferment of the early degradation process of the nanocomposites.	105

thermal conductivity and electrical conductivity of the blend composites depends on the dispersion of the nanofiller, content of the BP blend, concentration of the nanofillers and its localization in the BP blend. Botlhoko et al[112] reported that the addition of 0.05 wt% of thermally exfoliated reduced graphene oxide (TERGO2) increased the thermal conductivity by 77.13%, whereas 0.1 and 0.25 wt% TERGO2 increased the thermal conductivity by 67.67 and 66.81%, respectively when compared to the neat BP blend (PLA/PCL). The improvement in thermal conductivity was attributed to the evenly dispersed TERGO2 particles in the minor phase of PCL, which increased thermal transportation because of strong interactions between the TERGO2 particles and polymer chains in the BP blend. For a similar study,[112] in the context of electrical resistivity, the addition of the TERGO2 particles increased the electrical resistivity values of the blend composites. The electrical resistivity values for 0.05 and 0.1 of TERGO2 were comparable to those of neat PLA. This was attributed to some poor electrical path continuities of the dispersed TERGO2 due to preferential localization. Sivanjineyulu and co-workers[66] reported higher values (viz., more than 10^{13} Ω/square) for BP blends and individual BPs (ie, PLA and PBS). The incorporation of less than 3 phr CNTs can form a semiconductive network structure in the blend composite. In their study, adding as little as 0.5 phr decreased the electrical resistivity to about 10^{8} Ω/square, emphasizing that the electrical-percolation threshold was obtained at lower CNT's content. The authors also discovered that the selective localization of the CNTs had a significant effect on the electrical resistivity of the BP blend system. Poly(butylene succinate)/polylactide/polybutylene succinate-co-lactate/3 phr CNTs (PBS/PLA/PBSL/CNT) showed lower electrical resistivity when compared with CNTs-incorporated in PLA (PLA-T3) and CNT-added PBS (PBS-T3) with the same CNT content. The behavior was attributed to a uniform distribution of the CNTs in the PBS continuous phase, that is, selective localization in the composites resulted in double percolation threshold. Controlling the nanofiller localization at the interface between the two BP phases had a significant impact on the thermal conductivity of the resultant BP blend nanocomposite.[70] According to Huang and co-workers,[70] confining the graphene nanofiller sheets (GE) at the interface between PCL/PLA blend had a significant improvement on the thermal conductivity of the blend. PCL/PLA/0.53 vol% GE with different PLA concentration was prepared by the adsorption-desorption of polymer chains on the graphene surface.[70] The authors reported an increase in thermal conductivity at a co-continuous blend composition of the PCL/PLA with 0.53 vol% of graphene trapped at the interface (Figure 4).

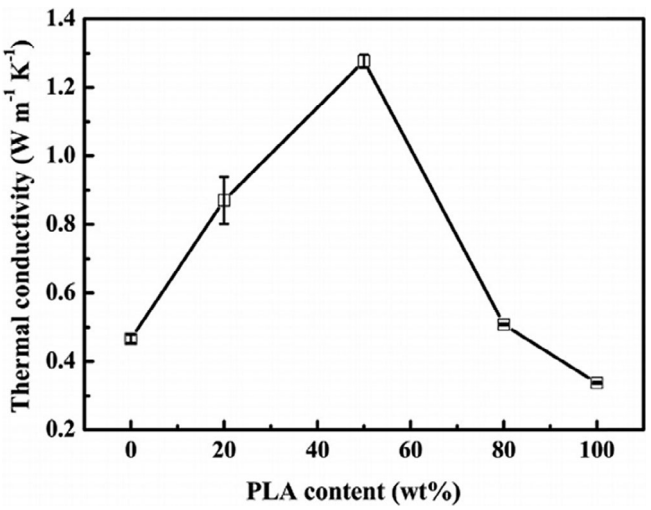

FIGURE 4 Thermal conductivities of PCL/PLA/0.53 vol% GE composites at different PLA contents.[70] Copyrights Elsevier. PCL, poly(caprolactone); PLA, poly(lactic acid)

9 | SHAPE MEMORY BEHAVIOR FOR BP BLEND COMPOSITES

In a scientific hindsight, the shape recovery (SR) property is the ability of the polymer material to retain its original shape after the release of the external stimuli[113] such as strenuous strain, temperature, pH, water, magnetic field, electricity, light, and/or humidity. In actuality, a stable "permanent region" of the material is required for the recollection of the original shape and a "switchable region" is also necessary to recover and for fixity of the original and temporary shapes, respectively. Shape memory behavior of the BP blend is an indispensable feature on the characteristics of both pristine BP blends and their nanocomposite versions for the betterment of their applicability.[114,115] SR for polymers is, in general, beneficial in various technological applications especially in biomedical field for the minimally invasive surgeries.[116,117] It is well known that the formation of BP blends using individual BP materials by blending provides an outstanding enhancement of the most important properties of the resultant BP hybrids. Moreover, the incorporation of the foreign particulates into the BP blends furnishes a considerable improvement on the properties of the BP blend nanocomposites wherein the extent of applicability can be broadened as a result. The SR properties of the BPs blend composites have found the great deal of utility in the biomedical, textile, aerospace and other applications in various fields of more recent technological aspects. In particular, the utilization of shape memory BP blend composites comprising a shape memory effect (SME) as the implant scaffolds for the regeneration/replacement of the defect of mammalian tissues has gained more interest in the field of biomedicine.[118]

Due to various aforementioned external stimuli factors by which the shape memory materials would experience the SME, different studies have been conducted in recent years wherein an ascertainment of the SR materials under dissimilar conditions was the subject of interest. However, the scope of the current review will be restricted particularly on the shape memory effect of the BP-based blend composites comprising different compositions of BP-based blends of various BPs. The temperature range in which the resultant BP blend composites are treated plays a crucial role and the literature data revealed that excessively higher temperatures could lead to the delamination of scaffolds that culminate to the degradation of the materials. The effect of temperature and the compatibility between the bio(polymer) materials as well as the extent of dispersion of the filler are ordinarily considered as the centerpieces in the entire concept of SR especially for the BP blend composites. The filler content influences the extent of shape memory recovery of the films of the BP-based blend composites. For instance, Liu and coworkers[114] investigated the effect of the different contents of SiO_2 nanoparticles on to the polylactide blended with natural rubber denoted by PLA/NR/SiO_2 prepared using the melt compounding method. As shown in Figure 5, the SR increased to the highest at 15 wt% of the SiO_2 nanoparticles and diminishes gradually with a further increase of the content of the nanofiller. It was deduced that the increase of the nanofiller to higher content in resulted in the agglomeration of particles that culminated in the decrease of the SR of the PLA/NR/SiO_2 films. The authors emphasized that the natural rubber phase was the key region for SR of the BP-based blend nanocomposites whereas the PLA phase accounted for the shape memory effect and fixed the deformed rubber phase at room temperature.

Shape memory properties vs degree of compatibility between the components of the blend of the BP blend composites was investigated by Sessini and coworkers.[86] The authors discovered that the thermally activated shape memory response was not influenced by the incorporation of the CNCs into the PLA and poly(ε-caprolactone) (PCL) blend, but slightly affected by the compatibility amongst the components of the blend and the values for both strain recovery ratio and strain fixity ratio were higher than 80% and 98%, respectively. The following Equations (4 and 5) were employed in the determination of recovery and fixity ratios of the investigated BP blend composites (PLA/PCL/CNC), accordingly:

$$R_r(N) = \frac{\left(\varepsilon_m - \varepsilon_p(N)\right)}{\left(\varepsilon_m - \varepsilon_p(N-1)\right)} \times 100\% \quad (4)$$

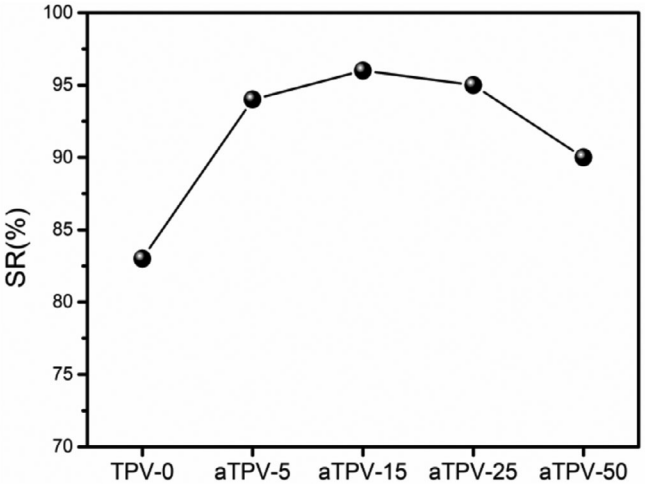

FIGURE 5 Shape recovery ratio of a TPVs with various SiO_2 nanoparticles content.[114] Copyrights Elsevier

$$R_f(N) = \frac{\varepsilon_u(N)}{\varepsilon_m} \times 100\% \quad (5)$$

where, ε_m is the deformed strain, ε_u the fixed strain, ε_p the recovered strain, and N is the number of cycles.

As mentioned previously, the range of temperature within which the shape memory response is evaluated forms an integral part of the concept of SR in its entirety leading to the development of smart polymer materials for use in modern communities. Any temperature above the glass transition temperature (T_g) of pristine components of BP blend accounts for the sample to be interchangeably turned into various shapes as a result of softening effect. This intriguing phenomenon of thermo-activated shape memory response is visually demonstrated in the work performed by Cao and coworkers.[119] The specimens of BP-based blend composites consisting of PLA, epoxidized natural rubber and CNC were prepared by melt compounding method using internal mixer at 155°C followed by compressing molding at 170°C. The composites showed an effortless deformation to produce various shapes under warm water bath at 70°C and the obtained shape was readily fixed at the temperature close to 20°C (an ambient temperature). The authors perceived no shape resilience within 24 hours, however, when the specimens were immersed into warm water (70°C), an instantaneous (roughly 10 seconds) revert from deformed shape to original shape was observed as visually depicted in Figure 6.

Quite fascinating results regarding the shape memory response were reported by Peponi and coworkers[96] the 3D diagrams for thermos-mechanical cycles. Figure 7 shows the thermo-mechanical cycles of PLA/PCL/ nanosized hydroxyapatite nanocomposites prepared by extrusion process at 180°C and subsequent compression molding at an equivalent temperature. It is clearly observed in the 3D diagrams that the SR of all samples was achieved at 55°C and the capability to return to initial shape. Also, the BP blend nanocomposites show the ability to sustain temporary deformed shape and to recover to original shape.

10 | INFLUENCE OF NANOFILLERS ON BARRIER PROPERTIES OF BIODEGRADABLE POLYMER BLENDS

Nanoclay and graphene are widely used for enhancing the barrier properties of polymers. Nanoclays are nanoparticles made from layered mineral silicates that have a stacked structure of 1 nm silicate sheets. Figure 8 shows typical schematic sketches of polymer/clay nanocomposites (PCNs), transmission electron microscope (TEM) images, and their X-ray diffraction (XRD) patterns. The morphology of the PCNs is generally classified into immiscible, intercalated, or exfoliated. The TEM image in Figure 8 for immiscible PCN shows that clay platelets agglomerate to form large tactoids which are phase separated from the polymer matrix. Moreover, the XRD peak of clay in the composite is at the same position as that of neat clay suggesting that the polymer chains are unable to separate the clay platelets in immiscible composites. Immiscible composites are commonly produced when hydrophobic polymers are mixed with unmodified or organically modified nanoclay due to the lack of thermodynamic interactions between the polymer and polar aluminosilicate surface of nanoclay.[121] In intercalated PCNs, the polymer chains have entered the clay galleries and separated the platelets resulting in increased interlayer spacing between the platelets. The XRD peaks of intercalated PCNs occur at lower angles than those of neat clay indicating expansion of the gallery. The dispersion of clay in intercalated PCNs is better than in the immiscible PCNs. There is no stacking pattern of nanoclay platelets in exfoliated PCN in Figure 1 and the XRD spectrum is featureless due to irregular spacing of the platelets. The clay content of an exfoliated

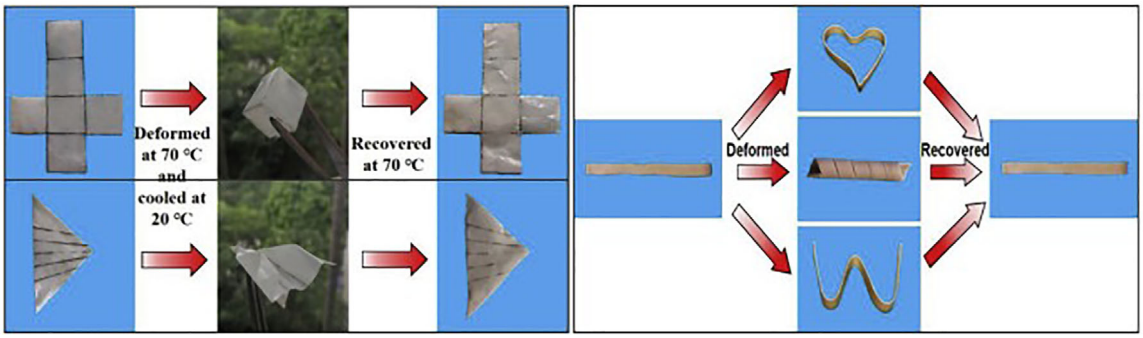

FIGURE 6 Visual illustration of shape memory behavior of the TPVs.[119] Copyrights Elsevier [Color figure can be viewed at wileyonlinelibrary.com]

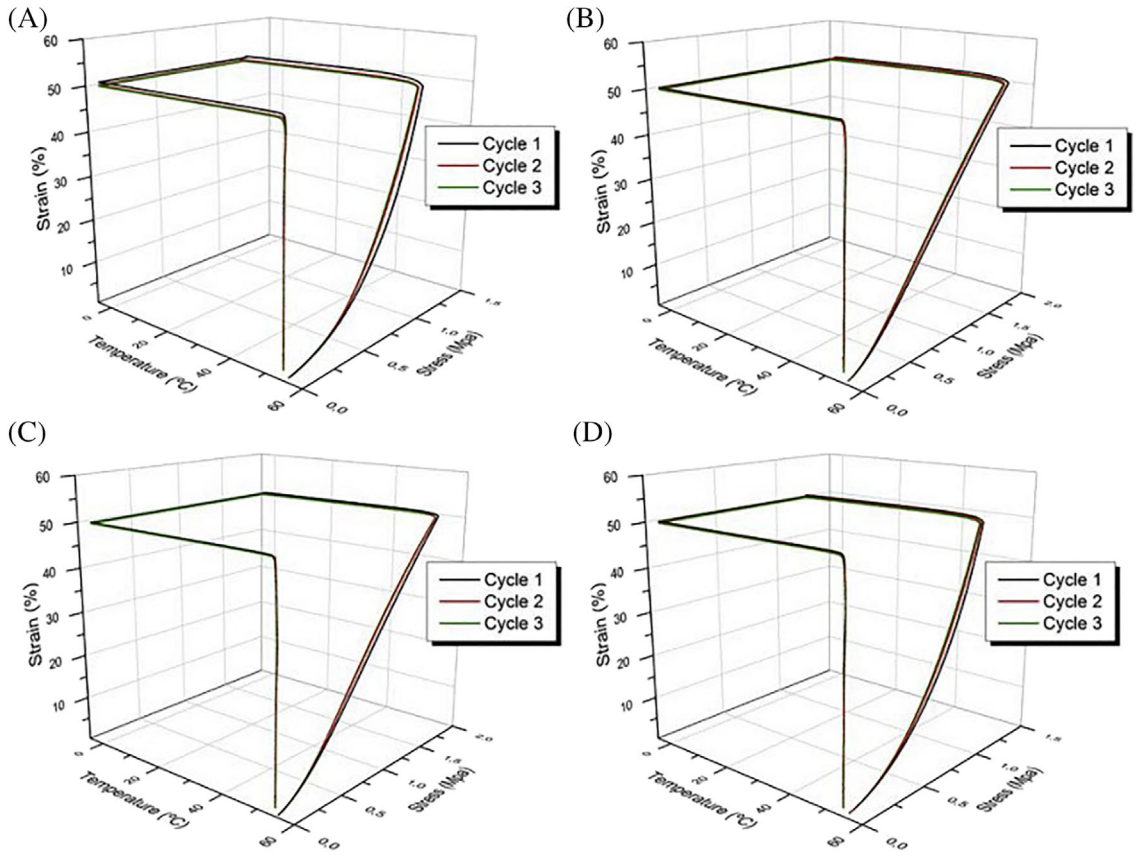

FIGURE 7 Legend on next page.

nanocomposite is usually much lower than that of intercalated nanocomposite.[122] The completely exfoliated PCNs are more fancied than other composites for applications such as packaging because they provide superior gas and water vapor barrier properties. The superior barrier properties in exfoliated PCNs as depicted in Figure 9 are attributed to the exfoliated clay platelets which form a tortuous path.[122]

The size of the graphene and graphene oxide platelets, stacking orientation, and degree of graphene exfoliation in the polymer matrix are factors which determine the gas transport.[124] The relatively higher aspect ratio of graphene-based 2D materials provides much longer pathways for penetration of gas molecules than other nanofillers, provided they are fully exfoliated and well dispersed in polymer nanocomposites.[120] In the literature, a lot of work has been reported on gas barrier properties of binary biodegradable polymer nanocomposites, but only few studies report on the gas barrier properties of ternary biodegradable polymer nanocomposites.[125–129] Sabet et al reported on the effect of clay (DK2) on the oxygen (O_2) barrier properties of PLA/PCL blends compatibilized with different compatibilizers containing varying levels of maleation, (licocene with 7% maleic anhydride), and (polybond with 1% maleic anhydride).[125] The O_2 barrier of the PLA/PCL blend was enhanced with incorporation of DK2, but a combination of DK2 and polybond in the PLA/PCL blend resulted in superior barrier properties than when licocene is used instead of polybond in the mixture. The better O_2 barrier of PLA/PCL/polybond/DK2 composite was attributed to longer and flocculated dispersed silicate layers which enlarged the diffusing path, whereas the relatively low O_2 barrier of PLA/PCL/licocene/DK2 composite was attributed to licocene, which has a lubricating effect in the melt and retards the packing of the PCL and PLA chains during the quenching process. Bhatai et al investigated the effect of incorporating increasing amounts (1-10 wt%) of clay (C30BX) on the O_2 permeability of PLA/PBSA blend.[126] An optimum reduction, that is, 26% reduction of O_2 permeability relative to the pristine PLA/PBSA blend was achieved with incorporating about 3 wt% C30BX. The authors attributed the reduction of O_2 permeability to the combination of the increased crystallinity due to the presence of clay and the small decrease in void density. Ojijo et al used two types of clays (C20A and MEE) which have different aspect ratio in the presence of chain extender, triphenyl phosphite to investigate their effect on the gas

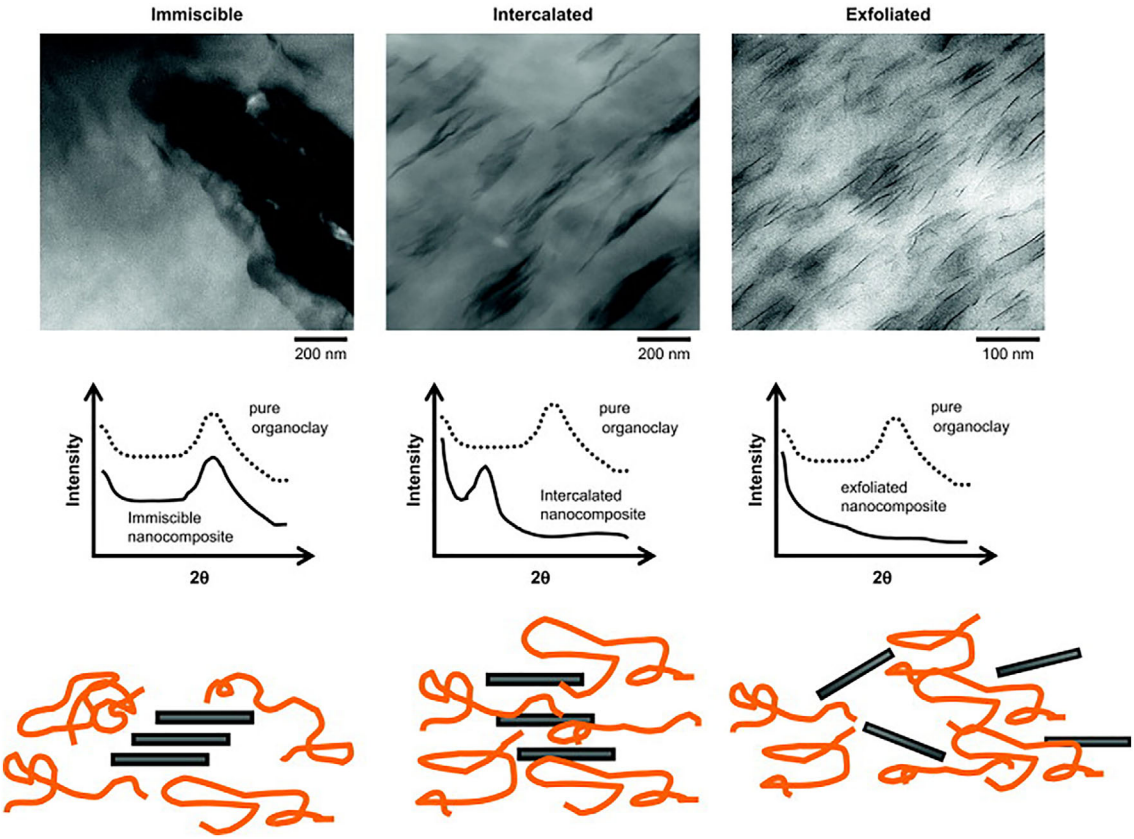

FIGURE 8 Typical morphologies of polymer/clay nanocomposites (PCNs).[120] Copyrights Elsevier [Color figure can be viewed at wileyonlinelibrary.com]

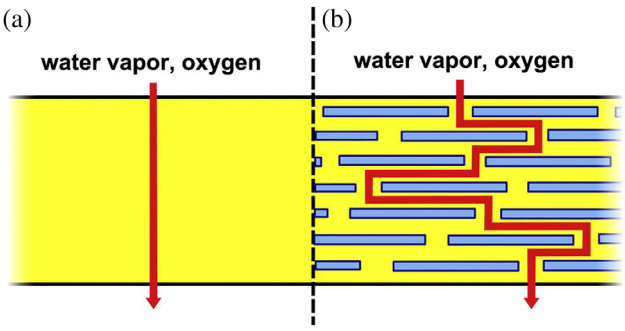

FIGURE 9 Illustration of the "tortuous pathway" created by incorporation of exfoliated nanoclay platelets into a polymer matrix film. In a pristine polymer film polymer, A, diffusing gas, water vapor molecules migrate via a pathway that is perpendicular to the film orientation. In a polymer/clay nanocomposite (PCN), B, diffusing gas and water vapor molecules navigate around impenetrable nanoclay platelets and through interfacial zones which have different permeability characteristics than those of the pristine polymer.[123] Copyrights Elsevier [Color figure can be viewed at wileyonlinelibrary.com]

and water vapor barrier properties of PLA/PBSA.[127] At equal composition, the MEE clay showed superior enhancement in the barrier properties compared to the C20A and this was attributed to the larger aspect ratio of MEE and better crystallinity of the PLA component in MEE-based compatibilized blends resulting in close packing of the polymer chains. Yang et al plasticized PLA by blending PLA with low molecular weight PBSA and coupling PBSA to carboxylic-functionalized PLA and investigated its barrier properties.[128] The PLA/PBSA blend showed higher O_2 permeability than pristine PLA and this was attributed to phase separation in the blend and low T_g of the PLA phase. However, the PLA-CA-PBSA had lower O_2 permeability than both pristine PLA and the PLA/PBSA blend. The authors attributed the lower O_2 permeability of PLA-CA-PBSA to the combination of higher degree of crystallinity and space filling and better miscibility. Boukaz et al used a combination of clay and epoxy functionalized graphene to investigate their effect on the barrier properties of PLA/PCL blend.[129] The incorporation of 3 wt% epoxy functionalized graphene in the PLA/PCL blend had no significant effect on water vapor permeability and this was attributed to the poor dispersion of graphene in the blend. However, incorporating clay alone in the blend reduced the water vapour permeability and this was linked to the dispersion state of clay, which played an important role in delaying the diffusion

of the gas molecules in the polymers matrices. The water vapor permeability of the PLA/PCL blend reduced further when a combination of 3 wt% epoxy functionalized graphene and 3 wt% nanoclay were incorporated. These results were attributed to the existence of the high diffusion pathway for water vapor molecules in the matrix, as a consequence to the high level of co-dispersion of the nanofiller mixtures (organomontmorillonite and graphene).[129]

Although research was done to investigate the influence of nanofillers on the gas and water vapor barrier properties of biodegradable blends, to our knowledge no work has been reported which investigates the influence of selectively localizing nanofillers in different phases of biodegradable blends on barrier properties of the same. Therefore, our research group is currently exploring that topic.

11 | CONCLUSION AND FUTURE REMARKS

The development of innovative BP blend-nanofillers composites has resulted in novel materials with specialized properties, which are mainly dependent on the type of modified nanofillers and synthesis approach. In general, melt blending is considered to be an industrially viable, as well as an eco-friendly synthesis approach. The *in-situ* polymerization technique delivers more control of the synthesis process in terms of the grafted amounts of organic solvents, the nanofillers interlayer spacing and the dispersion of nanoclays in the VP blend matrix. Three different synthesis methods and their impact on the structure and properties of BP blend-nanofillers composites were discussed in this review article. Applications of polymer-nanoclay composites have gained momentum and these composites show promise in a wide range of innovative applications. This review article presents recent developments in novel polymer-nanoclay composites with potential applications in various industries, such as petroleum, food packaging, biomedical, and wastewater treatment. Some composites exhibit excellent reinforcement characteristics for physicochemical properties of materials. The process of selecting combinations of BP blends and nanofillers to design and synthesize composites appears to be without a well-established scientific principle. Thus, the theory and modeling related to the design of BP blend-nanoclay composites may require additional focus to provide a better understanding of high-performance composites. It is estimated that by 2020, the demand for novel BP blend-nanofillers composite materials is likely to increase to about 3.2 million tons and at a cost of US$ 15 billion per year. Major areas of application for future novel BP blend-nanofillers composites are likely to include health (biomedical applications), safety (food packaging), and the environment (biodegradable materials).

ACKNOWLEDGMENTS

The National Research Foundation of South Africa is acknowledged for financial support.

ORCID

Mokgaotsa J. Mochane https://orcid.org/0000-0002-4805-2198

Teboho C. Mokhena https://orcid.org/0000-0003-2153-3845

REFERENCES

[1] B. Kunwar, H. N. Cheng, S. R. Chandrashekaran, B. K. Sharma, *Renew. Sust. Energy Rev.* **2016**, *54*, 421.
[2] M. Lackner, *Bioplastics-biobasedplastics as renewable alternatives to petroplastics*. In: Kirk-Othmer Encyclopedia of Chemical Technology, 6th ed., New York, USA, Wiley, **2015**, p.1.
[3] Y. Weldemichael, G. Assefa, *J. Clean. Prod.* **2016**, *112*, 4257.
[4] N. Gaurav, S. Sivasankari, G. S. Kiran, A. Ninawe, J. Selvin, *Renew. Sust. Energy Rev.* **2016**, *73*, 205.
[5] U. Neuling, M. Kaltschmitt, *J. Oil Palm. Res.* **2017**, *29*, 137.
[6] S. Parka, E. Liha, K. Parka, Y. K. Jounga, D. K. Han, *Prog. Polym. Sci.* **2017**, *68*, 77.
[7] K. M. Zia, A. Noreen, M. Zuber, S. Tabasum, M. Mujahid, *Int. J. Biol. Macromol.* **2016**, *82*, 1028.
[8] R. Scaffaro, A. Maio, F. Sutera, E. F. Gulino, M. Morreale, *Polym.* **2019**, *11*, 651.
[9] M. P. Arrieta, M. D. Samper, M. Aldas, J. Lopez, *Materials* **2017**, *10*, 1.
[10] A. Noreen, K. M. Zia, M. Zuber, M. Ali, M. Mujahid, *Int. J. Biol. Macromol.* **2016**, *86*, 937.
[11] A. Arevalo-Gallegos, Z. Ahmad, M. Asgher, R. Parra-Saldivar, H. M. N. Iqbal, *Int. J. Biol. Macromol.* **2017**, *99*, 308.
[12] I. Manavitehrani, A. Fathi, H. Badr, S. Daly, A. N. Shirazi, *Polym.* **2016**, *8*, 1.
[13] K. Nazemi, P. Azadpour, F. Moztarzadeh, A. M. Urbanska, M. Mozafari, *Mater. Lett.* **2015**, *138*, 16.
[14] I. Manavitehrani, A. Fathi, Y. Wang, P. K. Maitz, F. Dehghani, *ACS Appl. Mater. Interfaces* **2015**, *7*, 22421.
[15] X. Guo, L. Wang, X. Wei, S. Zhou, *Polym. Chem.* **2016**, *54*, 3525.
[16] P. Davoodi, L. Y. Lee, Q. Xu, V. Sunil, Y. Sun, S. Soh, C. H. Wang, *Adv. Drug Delivery Rev.* **2018**, *132*, 104.
[17] T. Fuoco, D. Pappalardo, A. Finne-Wistrand, *Macromolecules* **2018**, *50*, 7052.
[18] X. Li, X. Yan, J. Yang, H. Pan, G. Gao, H. Zhang, L. Dong, *Polym. Eng. Sci.* **2018**, *58*, 1868.
[19] B. V. M. Rodrigues, A. S. Silva, G. F. S. Melo, L. M. R. Vasconscellos, F. R. Marciano, A. O. Lobo, *Mater. Sci. Eng. C* **2016**, *59*, 782.
[20] L. F. Maldonado, P. A. R. Muñoz, G. J. M. Fechine, *J. Polym. Environ.* **2018**, *26*, 3187.

[21] M. P. Arrieta, E. Fortunati, F. Dominici, J. López, J. M. Kenny, *Carbohydr. Polym.* **2015**, *121*, 265.
[22] I. Armentano, E. Fortunati, N. Burgos, F. Dominici, F. Luzi, S. Fiori, A. Jiménez, K. Yoon, J. Ahn, S. Kang, J. M. Kenny, *eXPRESS Polym. Lett.* **2015**, *9*, 583.
[23] R. Muthuraj, M. Misra, A. K. Mohanty, *J. Appl. Polym. Sci.* **2015**, *132*, 421.
[24] R. Malinowski, *Int. J. Adv. Manuf. Tech.* **2016**, *87*, 3307.
[25] T. A. Oliveira, R. R. Oliveira, R. Barbosa, J. B. Azevedo, T. S. Alves, *Carbohydr. Polym.* **2017**, *168*, 52.
[26] K. Żółtowska, M. Sobczak, E. Olędzka, *Molecules* **2015**, *20*, 2816.
[27] Q. Yao, J. G. L. Cosme, T. Xu, J. M. Miszuk, P. H. S. Picciani, H. Fong, H. Sun, *Biomaterials* **2017**, *115*, 115.
[28] G. Turnbull, J. Clarke, F. Picard, P. Riches, L. Jia, F. Han, B. Li, W. Shu, *Bioact. Mater.* **2018**, *3*, 278.
[29] T. Ghassemi, A. Shahroodi, M. H. Ebrahimzadeh, A. Mousavian, J. Movaffagh, A. Moradi, *Arch. Bone Jt. Surg.* **2018**, *6*, 90.
[30] Y. Hu, W. A. Daoud, K. K. L. Cheuk, C. S. K. Lin, *Materials* **2016**, *9*, 133.
[31] J. Muller, C. González-Martínez, A. Chiralt, *Materials* **2017**, *10*, 952.
[32] R. Scaffaro, L. Botta, F. Lopresti, A. Maio, F. Sutera, *Cellulose* **2017**, *24*, 447.
[33] M. E. Inacio, D. H. S. Souza, M. L. Dias, *Mater. Sci. Appl.* **2020**, *11*, 44.
[34] E. Fortunati, D. Puglia, A. Iannoni, A. Terenzi, J. M. Kenny, L. Torre, *Materials* **2017**, *10*, 809.
[35] M. Shabina, M. Afzal, S. Hameed, *Green Chem. Lett. Rev.* **2015**, *8*, 56.
[36] J. Lim, M. You, J. Li, Z. Li, *Mater. Sci. Eng. C* **2017**, *79*, 917.
[37] S. Ghysels, M. S. I. Mozumder, H. De Wever, E. I. P. Volcke, L. Garcia-Gonzalez, *Bioresour. Technol.* **2018**, *249*, 858.
[38] K. Müller, E. Bugnicourt, M. Latorre, M. Jorda, Y. E. Sanz, J. M. Lagaron, O. Miesbauer, A. Bianchin, S. Hankin, U. Bölz, G. Pérez, M. Jesdinszki, M. Lindner, Z. Scheuerer, S. Castelló, M. Schmid, *Nanomaterials* **2017**, *7*, 1.
[39] K. Susheela, I. Satyanarayana, *Int. J. Mod. Eng. Res. Technol.* **2018**, *5*, 1.
[40] G. P. da Silva, C. J. B. Lima, J. Contiero, *Catal. Today* **2015**, *257*, 259.
[41] C. Leopold, T. Augustin, T. Schwebler, J. Lehmann, W. V. Liebig, B. Fiedler, *J. Colloid Interface Sci.* **2016**, *506*, 620.
[42] K. Li, S. Jin, X. Liu, H. Chen, J. He, J. Li, *Polymer* **2017**, *9*, 247.
[43] S. Gul, A. Kausar, M. Mehmood, B. Muhammad, S. Jabeen, *Polym. Plast. Technol. Eng.* **2016**, *55*, 18421.
[44] Y. Yin, R. Huang, W. Zhang, M. Zhang, C. Wang, *Chem. Eng. J.* **2016**, *289*, 99.
[45] B. N. Sahoo, K. Balasubramanian, *RCS Adv.* **2015**, *5*, 6743.
[46] S. N. Tripathi, G. S. S. Rao, A. B. Mathur, R. Jasra, *RSC Adv.* **2017**, *7*, 23615.
[47] I. Ahmad, B. Yazdani, Y. Zhu, *Nanomaterials* **2015**, *5*, 90.
[48] S. Nasir, M. Z. Hussein, Z. Zainal, N. A. Yusof, *Materials* **2018**, *11*, 1.
[49] Y. Zhang, J. Chen, C. Xu, K. Zhou, Z. Wang, J. Zhou, K. Cen, *Int. J. Hydrogen Energy* **2016**, *41*, 2215.
[50] U. P. Shaik, D. D. Purkayastha, M. G. Krishna, V. Madhurima, *Appl. Surf. Sci.* **2015**, *330*, 292.
[51] C. Pramanik, J. R. Gissinger, S. Kumar, H. Heinz, *ACS Nano* **2017**, *11*, 12805.
[52] E. Kabir, V. Kumar, K. H. Kim, A. C. K. Yip, J. R. Sohn, *J. Environ. Manag.* **2018**, *225*, 261.
[53] Y. Wang, X. Xu, J. Dai, J. Yang, T. Huang, N. Zhang, Y. Wang, Z. Zhou, J. Zhong, *RSC Adv.* **2014**, *4*, 59194.
[54] C. Liu, F. Ma, Z. Zhang, J. Yang, Y. Yang, Y. Wang, Z. Zhou, *Compos. Part B* **2016**, *107*, 174.
[55] X. Wang, Z. Zhang, J. Li, J. Yang, Y. Wang, J. Zhang, *RSC Adv.* **2015**, *5*, 69522.
[56] X. Wang, Z. He, J. Yang, N. Zhang, T. Huang, Y. Wang, Z. Zhou, *Compos. Part A* **2016**, *91*, 105.
[57] J. Huang, C. Mao, Y. Zhu, W. Jiang, X. Yang, *Carbon* **2014**, *73*, 267.
[58] L. Shao, J. Dai, Z. Zhang, J. Yang, N. Zhang, T. Huang, Y. Wang, *RSC Adv.* **2015**, *5*, 101455.
[59] Y. Shi, W. Zhang, J. Yang, T. Huang, N. Zhang, Y. Wang, G. Yuan, C. Zhang, *RSC Adv.* **2013**, *3*, 26271.
[60] J. Chen, H. Lu, J. Yang, Y. Wang, X. Zheng, C. Zhang, G. Yuan, *Compos. Sci. Tech.* **2014**, *94*, 30.
[61] L. Bai, R. Sharma, X. Cheng, C. W. Macosko, *Langmuir* **2018**, *34*, 1073.
[62] C. Liu, F. Ma, Z. Zhang, J. Yang, Y. Wang, *Compos. Part B* **2017**, *123*, 1.
[63] T. Zhang, J. Yang, N. Zhang, T. Huang, Y. Wang, *Ind. Eng. Chem. Res.* **2017**, *56*, 3607.
[64] Y. Shen, T-T. Zhang, J-H. Yang, N. Zhang, T. Huang, Y. Wang, *Polym. Compos.* **2015**, *38*, 1982.
[65] O. C. Wokadala, S. S. Ray, J. Bandyopadhyay, J. W. Smith, N. M. Emmambux, *Polymer* **2015**, *71*, 82.
[66] V. Sivanjineyulu, K. Behera, Y. H. Chang, F. C. Chiu, *Compos. Part A* **2018**, *114*, 30.
[67] J. P. Mofokeng, A. S. Luyt, *J. Mater. Sci.* **2015**, *50*, 3812.
[68] Y. Ahmadzadeh, A. Babaei, A. Goudarzi, *Polym. Degrad. Stabil.* **2018**, *158*, 136.
[69] W. Wu, C. Wu, H. Peng, Q. Sun, L. Zhou, J. Zhuang, X. Cao, V. A. L. Roy, R. K. Y. Li, *Compos. Part B.* **2017**, *113*, 300.
[70] J. Huang, Y. Zhu, L. Xu, J. Chen, W. Jiang, X. Nie, *Compos. Sci. Technol.* **2016**, *129*, 160.
[71] S. E. Fenni, O. Monticelli, L. Conzatti, R. Doufnoune, P. Stagnaro, N. Haddaoui, D. Cavallo, *eXPRESS Polym. Lett.* **2018**, *12*, 58.
[72] J. P. Mofokeng, A. S. Luyt, *Thermochim. Acta.* **2015**, *613*, 41.
[73] A. S. Luyt, S. Gasmi, *J. Polym. Environ.* **2018**, *26*, 2410.
[74] J. G. Ausejo, J. G. Pérez, R. Balart, J. M. Lagarón, L. Cabedo, *Polym. Compos.* **2017**, *40*, E156.
[75] I. Zembouai, M. Kaci, L. Zaidi, S. Bruzaud, *Polym. Degrad. Stab.* **2018**, *153*, 47.
[76] I. Kelnar, J. Kratochvìl, L. Kaprálková, A. Zhigunov, M. Nevoralová, *J. Mech. Behav. Biomed. Mater.* **2017**, *71*, 271.
[77] O. J. Botlhoko, S. S. Ray, J. Ramontja, *Eur. Polym. J.* **2018**, *102*, 130.
[78] J. Esmaeilzadeh, S. Hesaraki, S. M. Hadavi, M. H. Ebrahimzadeh, M. Esfandeh, *Mater. Sci. Eng. C* **2017**, *77*, 978.
[79] P. Kanmani, J. W. Rhim, *Carbohydr. Polym.* **2014**, *106*, 190.

[80] N. Ghaemi, Z. Khodakarami, *Carbohydr. Polym.* **2019**, *204*, 78.
[81] B. J. Tiimob, V. K. Rangari, G. Mwinyelle, W. Abdela, P. G. Evans, N. Abbott, T. Samuel, S. Jeelani, *Food Packag. Shelf Life* **2018**, *15*, 9.
[82] R. A. Russell, L. J. R. Foster, P. J. Holden, *Eur. Polym. J.* **2018**, *105*, 150.
[83] J. Urquijo, N. Aranburu, S. Dagréou, G. Guerrica-Echevarríaa, J. I. Eguiazábal, *Eur. Polym. J.* **2017**, *93*, 545.
[84] M. El Achaby, N. El Miri, A. Aboulkas, M. Zahouily, E. Bilal, A. Barakat, A. Solhy, *Int. J. Biol. Macromol.* **2017**, *96*, 340.
[85] Z. Yu, F. K. Alsammarraie, F. X. Nayigiziki, W. Wang, B. Vardhanabhuti, A. Mustapha, M. Lin, *Food Res. Int.* **2017**, *99*, 166.
[86] V. Sessini, I. Navarro-Baena, M. P. Arrieta, F. Dominici, D. Lopez, L. Torre, J. M. Kenny, P. Dubois, J. M. Raquez, L. Peponi, *Polym. Degrad. Stab.* **2018**, *152*, 36.
[87] E. Campodoni, E. B. Heggset, A. Rashad, G. B. Ramírez-Rodríguez, K. Mustafa, K. Syverud, A. Tampieri, M. Sandri, *Mater. Sci. Eng. C* **2019**, *94*, 867.
[88] P. Wang, S. W. Tang, F. Sheng, J. Cai, P. Fei, A. Nawaz, N. Walayat, A. B. Javaid, H. Xiong, *Int. J. Biol. Macromol.* **2019**, *132*, 1208.
[89] M. El Achaby, Z. Kassaba, A. Barakat, A. Aboulkas, *Ind. Crop. Prod.* **2018**, *112*, 499.
[90] S. Shankar, J. W. Rhim, *Carbohydr. Polym.* **2018**, *196*, 92.
[91] M. C. Condes, M. C. Anona, A. Dufresne, A. N. Mauri, *Food Hydrocoll.* **2018**, *74*, 159.
[92] S. Mathew, S. Snigdha, J. Mathew, E. K. Radhakrishnan, *Appl. Clay Sci.* **2018**, *161*, 464.
[93] B. Rukmanikrishnan, S. S. Kim, J. Lee, J. Lee, *Int. J. Biol. Macromol.* **2019**, *123*, 1020.
[94] M. M. Rahmana, M. S. Islamb, G. S. Li, *Polym. Test.* **2018**, *68*, 302.
[95] S. Shankar, J. W. Rhima, K. Won, *Int. J. Biol. Macromol.* **2018**, *107*, 1724.
[96] L. Peponi, V. Sessini, M. P. Arrieta, I. Navarro-Baena, A. Sonseca, F. Dominici, E. Gimenez, L. Torre, A. Tercjak, D. López, J. M. Kenny, *Polym. Degrad. Stab.* **2018**, *151*, 36.
[97] Z. Li, J. K. Muiruri, W. Thitsartarn, X. Zhang, B. H. Tan, C. He, *Compos. Sci. Technol.* **2018**, *159*, 11.
[98] S. Adrar, A. Habi, A. Ajji, Y. Grohens, *Appl. Clay Sci.* **2018**, *157*, 65.
[99] Y. H. Yun, H. G. Youn, J. Y. Shin, S. D. Yoon, *Int. J. Biol. Macromol.* **2017**, *104*, 1150.
[100] S. Sharmeen, A. F. M. M. Rahman, M. M. Lubna, K. S. Salem, R. Islam, M. A. Khan, *Bioact. Mater.* **2018**, *3*, 236.
[101] Y. Zare, K. Y. Rhee, *Compos. Part B* **2019**, *158*, 162.
[102] R. Ma, Y. Wang, H. Qi, C. Shi, G. Wei, L. Xiao, Z. Huang, S. Liu, H. Yu, C. Teng, H. Liu, V. Murugadoss, J. Zhang, Y. Wang, Z. Guo, *Compos. Part B* **2019**, *167*, 396.
[103] A. Shah, M. Ali Buabeid, E. A. Arafa, I. Hussain, L. Lid, G. Murtaza, *Int. J. Pharm.* **2019**, *564*, 22.
[104] I. Zia, S. Mirza, R. Jolly, A. Rehman, R. Ullah, M. Shakir, *Int. J. Biol. Macromol.* **2019**, *124*, 88.
[105] D. Makwana, J. Castaño, R. S. Somani, H. C. Bajaj, *Arab. J. Chem.* **2020**, *13*, 3092.
[106] T. Huang, J. Li, J. Yang, N. Zhang, Y. Wang, Z. Zhou, *Compos. Part B* **2018**, *133*, 177.
[107] H. Tian, K. Wang, D. Liu, J. Yan, A. Xiang, A. V. Rajulu, *Int. J. Biol. Macromol.* **2017**, *101*, 314.
[108] S. Bonardd, M. Schmidt, M. Saavedra-Torres, A. Leiva, D. Radic, C. Saldías, *Carbohydr. Polym.* **2016**, *144*, 315.
[109] M. P. Arrieta, L. Peponi, D. López, M. Fernández-García, *Ind. Crop. Prod.* **2018**, *111*, 317.
[110] X. Wang, Y. Gao, X. Li, Y. Xu, J. Jiang, J. Hou, Q. Li, L. S. Turng, *Polym. Test.* **2017**, *59*, 396.
[111] H. Moustafa, H. Galliard, L. Vidal, A. Dufresne, *Eur. Polym. J.* **2017**, *87*, 188.
[112] O. J. Botlhoko, J. Ramontja, S. S. Ray, *Polymer* **2018**, *139*, 188.
[113] Z.-X. Zhang, J.-X. Dou, J.-H. He, C.-X. Xiao, L.-Y. Shen, J.-H. Yang, Y. Wang, Z.-W. Zhou, *J. Mater. Chem. C* **2017**, *5*, 4145.
[114] Y. Liu, J. Huang, J. Zhou, Y. Wang, L. Cao, Y. Chen, *Mater. Chem. Phys.* **2020**, *242*, 122538.
[115] P. Xu, P. Ma, X. Cai, S. Song, Y. Zhang, W. Dong, M. Chen, *Eur. Polym. J.* **2016**, *84*, 1.
[116] S. Petisco-Ferrero, A. Etxeberria, J. R. Sarasua, *J. Mech. Behav. Biomed. Mater.* **2017**, *71*, 372.
[117] J. Liu, L. Sun, W. Xu, Q. Wang, S. Yu, J. Sun, *Carbohydr. Polym.* **2019**, *207*, 297.
[118] A. Gupta, A. Maharjan, B. S. Kim, *Appl. Sci.* **2019**, *9*, 4694.
[119] L. Cao, C. Liu, D. Zou, S. Zhang, Y. Chen, *Carbohydr. Polym.* **2020**, *230*, 115618.
[120] D. R. Paul, L. M. Robeson, *Polymer* **2008**, *49*, 3187.
[121] S. Hotta, D. R. Paul, *Polymer* **2004**, *45*, 7639.
[122] S. S. Ray, M. Okamoto, *Prog. Polym. Sci.* **2003**, *28*, 1539.
[123] T. V. Duncan, *J. Colloid. Interf. Sci.* **2011**, *363*, 1.
[124] B. M. Yoo, H. J. Shin, H. W. Yoon, H. B. Park, *J. Appl. Polym. Sci.* **2014**, *131*, 39628.
[125] S. S. Sabet, A. A. Katbab, *J. Appl. Polym. Sci.* **2009**, *111*, 1954.
[126] A. Bhatia, K. Kupta, S. N. Bhattacharya, H. J. Choi, *Intern. Polymer Process. XXV* **2010**, *1*, 5.
[127] V. Ojijo, S. S. Ray, R. Sadiku, *Macromol. Mater. Eng.* **2014**, *299*, 596.
[128] X. Yang, H. Xu, K. Odelius, M. Hakkarainen, *Materials* **2016**, *9*(1), 313.
[129] B. S. Bouakaz, A. Habi, Y. Grohens, I. Pillin, *Appl. Clay Sci.* **2017**, *139*, 81.

How to cite this article: Mochane MJ, Sefadi JS, Motsoeneng TS, Mokoena TE, Mofokeng TG, Mokhena TC. The effect of filler localization on the properties of biopolymer blends, recent advances: A review. *Polymer Composites*. 2020;1–22. https://doi.org/10.1002/pc.25590